An Assessment of the Unprotected LOF Accident at EOC-4 in the CRBRP Heterogeneous Core Design

by

J. E. Cahalan
F. E. Dunn
E. E. Gruber
J. M. Kramer
E. E. Morris
D. P. Weber
H. U. Wider

December 1982

Reactor Analysis and Safety Division
Argonne National Laboratory
9700 South Cass Avenue
Argonne, Illinois 60439

An Assessment of the Unprotected LOF Accident in the CRBRP Heterogeneous Core Design

by

J. E. Cahalan
F. E. Dunn
E. E. Gruber
J. M. Kramer
E. E. Morris
D. P. Weber
H. U. Wider

ABSTRACT

The hypothetical unprotected loss-of-flow (LOF) accident for the Clinch River Breeder Reactor (CRBR) with a heterogeneous core design has been investigated with the SAS3D whole core accident analysis computer code. The representation of critical phenomenology with experimentally validated models has played an essential role in this best estimate analysis of the LOF scenario. Fuel motion has been modeled consistently with the TREAT in-pile experiments L6 and L7, which were designed and executed to examine fuel disruption and dispersal under loss-of-flow conditions at elevated power. Molten cladding motion has been modeled consistently with TREAT experiments R4

and R5 and SLSF experiment P3A, which were designed and executed to examine coolant boiling, vapor dynamics, and cladding relocation. The effects of plenum fission gas were modeled on the basis of TREAT experiment R8, the only in-pile experiment for LOF simulation with significantly pressurized fission gas plena simulating end-of-life conditions. Fission gas distributions within the fuel matrix were examined with the fission gas migration model, FRAS3, validated against HEDL fission gas release (FGR) experiments. Finally, irradiated cladding failure under plenum gas pressurization was modeled on the basis of the HEDL FCTT experiments.

The whole core best estimate analyses show, with such experimentally validated models, a mild power burst with near zero energetics. This conclusion is valid even in the unlikely event that the plenum fission gas can act to compress the disrupting fuel. Parametric variation on clad failure and plenum gas release, and molten cladding relocation show very small sensitivities in initiating phase energetics. The potential for significant energetics appears to require pessimistic phenomenological modeling that is not supported by the present experimental database, and is therefore beyond that appropriate for a realistic assessment of the accident energetics. The likelihood of energetics approaching the Structural Margin Beyond the Design Base (SMBDB) value is very remote.

TABLE OF CONTENTS

	Page
I. INTRODUCTION	1
II. PHENOMENOLOGICAL CONSIDERATIONS	8
II.1 MODELING OF PLENUM GAS BLOWDOWN IN R8	10
II.2 EXPERIMENTAL RESULTS ON CLAD RELOCATION DYNAMICS	24
II.3 CLADDING FAILURE CRITERIA	30
III. EOC-4 LOF SUMMARY	34
IV. CONCLUSIONS	50
Appendix A: Modifications to the SAS3D Boiling Module to Account for Release of Plenum Gas into a Boiling Region	51
Appendix B: Two-Fluid Model Analyses of Plenum Fission Gas Release	57
Appendix C: SAS3D Modification to TREAT R-Series Coolant Hydraulics	70
Appendix D: Calculation of Plenum Blowdown Coupled with Pressure-Driven Fuel Motion	72
Appendix E: Modified Treatment of Partial Clad Blockages in the SAS3D Boiling Model	77
REFERENCES	79

LIST OF FIGURES

Figure	Title	Page
1	R8 Gas Plenum Blowdown	12
2	R8 Coolant Flow Rates, Flooded Friction Factor in CLAZAS	14
3	R8 Coolant Flow Rates, Nominal Single Phase Friction Factor in CLAZAS	15
4	Coolant Pressure Profile at the Onset of Clad Motion	18
5	Vapor Mass Flux at the Onset of Clad Motion	19
6	Coolant Pressure Profile After a Re-entry Event	20
7	R8 Clad Motion, Flooded Friction Factor in CLAZAS	21
8	R8 Clad Motion, Nominal Single Phase Friction Factor in CLAZAS	23
9	R5 Inlet Flow-rate Comparison	26
10	Sketch of the Voiding Pattern in the Reactor Core at the end of Case 1	44
B1	Rupture Site Pressure History Comparison	59
B2	TWOFLU Predicted Channel Pressure Distribution History	61
B3	TWOFLU Predicted Fission Gas Distribution History	62
B4	Lower Sodium Slug Interface Comparison	65
B5	PLUTO2 Predicted Channel Pressure Distribution History	66
B6	PLUTO2 Predicted Fission Gas and Sodium Vapor Mass History	68
D1	Assumed Simplified Geometry of the Pin Stub and Plenum Region	73

LIST OF TABLES

No.	Title	Page
1	Active Core Region (36 inch) Material Worth at EOC-4, Dollars.....	3
2	Timing of Events in the R8 Test.....	13
3	Timing of Cladding Events in P3A Experiment.....	29
4	Heating Rates for SAS3D Best Estimate LOF Case.....	31
5	Event sequence for Case 1.....	36
6	Event sequence for Case 2.....	41
7	Comparison of times between initiation of gas release and the initiation of fuel motion in Cases 1 and 2.....	43
8	Event sequence for Case 3.....	46
9	Comparison of times between initiation of gas release and the initiation of fuel motion in Cases 1 and 3.....	48
10	Work-energies based on adiabatic expansions of super-saturated fuel to a final pressure of 1 atm.....	49

I. Introduction

In an assessment of energetics potential for an unprotected loss-of-flow (LOF) accident, several factors may be identified as playing critical roles in determining maximum reactivity and power levels. Included in this set are the factors which add positive reactivity, such as the sodium void contribution and relocation of cladding away from the active core region, and negative reactivity factors including axial expansion, Doppler feedback, and fuel disruption and dispersal under overpower conditions. An additional factor that has been postulated is the potential for adding positive reactivity due to compaction of disrupting fuel by the gas in the pressurized fission gas plenum. Although there are factors, which are summarized below, which appear to mitigate concern for this latter scenario, the potential for its effect motivated a reassessment of the expected scenario in the unprotected loss-of-flow scenario. This reassessment, provided in response to NRC Question CS760.178A3[1], demonstrated the importance of representing important phenomenology with experimentally consistent models. Specifically, it was shown that fuel disruption and dispersal under overpower conditions was the dominant phenomenological consideration governing the potential for initiating phase energetics for the neutronic and thermal-hydraulic model of the heterogeneous CRBRP core described in the Project's assessment of HCDA energetics[2]. Available experimental evidence on fission gas release from the HEDL FGR tests was used to validate the FRAS3 phenomenological code[3,4,5], which was then used to establish fuel pin conditions in the whole core analysis code, SAS3D. Similarly, data from TREAT in-pile LOF tests under overpower conditions, Tests L6 and L7[6,7,8], were used to calibrate the fuel dispersal modeling in the SLUMPY[9] fuel motion model of SAS3D. When such experimentally based modeling was used in the energetics assessment of the low sodium void worth core

described in reference 2, it was shown that very mild excursions and essentially zero energetics would be expected. It was also shown that sufficient time existed in the accident sequence to rupture the cladding, expel the stored gas, and eliminate the potential for compaction. It was noted, in addition, that because of the relatively low positive reactivity additions from sodium voiding and clad relocation ($1.23 for void reactivity and 28¢ for clad reactivity at the time of fuel motion initiation in the lead channel) that the system was sufficiently far from prompt critical (a net reactivity of 59¢ at fuel motion initiation) that the conclusions were quite insensitive to a range of modeling assumptions.

A further investigation of accident sequences in the unprotected LOF area was subsequently requested by the NRC Staff after review of the Project's reassessment of sodium void worth uncertainties and their implication on the potential for the loss-of-flow driven transient overpower (LOF'd'TOP) event. The uncertainty analysis was provided in response to question CS760.178A2[1] and was based on a large experimental data base. This assessment included analysis of over 100 critical experiments in LMFBR-type assemblies of CRBRP size or larger. The assessment demonstrated that the uncertainty in sodium void worth is not as large as is commonly perceived and resulted in a net uncertainty of 7.9% in the central core (positive reactivity) region, 11.3% in the external core (negative reactivity) region, and 20.7% in the axial and internal blanket regions. An additional fact, however, that came from this investigation was a more accurate assessment of the nominal worths for all materials, but, most importantly, the sodium void and cladding worths. Table 1 contains these material worths as used in the SAS3D analysis and a comparison of comparable information contained in reference 2 and used in the previously mentioned LOF assessment. Particularly important aspects of this

TABLE I. Active Core Region (36 inch) Material Worth at EOC-4, Dollars

SAS Channel Number	Assembly Type	Number of Assemblies	Flowing Sodium Material Worth		Steel (Clad and Wire Wrap) Material Worth	
			GEFR[a] 00523	Best[b] Estimate	GEFR-523	Best Estimate
1	B	7	.100	.142	-.173	-.247
2	F	21	.386	.454	-.986	-1.311
3	B	21	.330	.463	-.607	-.807
4	F	9	.160	.189	-.414	-.544
5	B	36	.559	.735	-1.029	-1.267
6	F	6	.085	.103	-.265	-.329
7	F	12	.165	.198	-.51	-.607
8	B	12	.125	.158	-.242	-.274
9	F	6	.027	.042	-.157	-.174
10	F	12	.113	.141	-.417	-.471
11	F	24	.366	.425	-1.027	-1.230
12	F	12	-.038	-.011	-.120	-.123
13	F	18	.116	.141	-.466	-.501
14	F	18	-.200	-.186	+.152	+.201
15	F	24	-.082	-.059	-.101	-.068
Driver		162	1.098	1.438	-4.31	-5.16
Internal Blankets		76	1.114	1.498	-2.05	-2.59
Total		238	2.212	2.936	-6.36	-7.75

a - β = 0.00340
b - β = 0.00323

reassessment are the increase in sodium void reactivity in the driver assemblies from $1.10 to $1.44 and an increase in the driver assembly steel worths (clad and wirewrap) from $4.31 to $5.16. Such increases in the elements which typically add positive reactivity to the system have several implications. It would be expected that the introduction of larger sodium void reactivity would increase the rate of increase of the reactor power and shorten the time scale for the initiation of fuel disruption. If stored plenum fission gas can, as hypothesized, act to compress disrupting fuel pins, the potentially shortened time scale would limit the time available for gas blowdown and increase the potential for fuel compaction. On the other hand, the decreased blowdown time also raises the possibility that released fission gas may be a significant force in affecting sodium vapor dynamics and may significantly mitigate the potential for clad relocation due to sodium vapor streaming. Also, shorter time scales would generally imply a higher retention of fission gas still within the fuel pin matrix. This gas is the main force which drives fuel disruption and dispersal under mild overpower conditions. Hence, the dispersive potential for fuel material may, in fact, increase. It is clear that several competing effects are present in this hypothetical accident sequence, so an assessment of the integrated effects has been performed using the whole core analysis code SAS3D.

In the assessment of accident energetics with the higher void worth values, it is expected that an increased sensitivity to modeling assumptions will be present. Relating modeling to available experimental information is essential. Such a detailed approach in the area of fuel disruption and dispersal modeling was undertaken in the previous assessment[1], but in other areas including fission gas plena rupture, fission gas effects on sodium vapor dynamics, and molten cladding relocation, experimentally inconsistent, and yet

conservative, assumptions were employed. Having established a sound basis for fuel motion modeling, this present reassessment of the LOF scenario allows an opportunity to develop a similar experimentally based description of the phenomena mentioned above.

In the second section of this report, the three important phenomenological areas -- modeling of fission gas blowdown, molten cladding relocation, and clad failure due to plenum fission gas -- are reviewed. In each of these areas, specific experimental evidence is available to guide phenomenological and integrated analysis modeling. The TREAT R-series[10,11] provides information on sodium vapor dynamics, clad relocation and plenum fission gas release and the SLSF P-series[12,13] provides further information in the first two of these areas. Modeling of these experiments with the SAS3D integrated analysis code and comparison of the results with data is discussed. In the area of clad failure, the HEDL FCTT[14-18] and FCTT/TUCOP[19] tests are used to establish appropriate criteria.

In the third section of this report, this experimentally consistent modeling capability is used in the whole core analysis of the CRBRP LOF HCDA. Important phenomenological issues within the whole core analysis context are highlighted and the expected power and reactivity conditions are given. The role of the plenum fission gas is also discussed. Also, recognizing that there is some uncertainty in this modeling, an indication of the sensitivity of the whole core analysis results to modeling phenomena such as clad failure and cladding relocation is provided.

In the appendices, we have provided an independent justification and a phenomenologically based discussion of several elements of modeling in the SAS3D code. In particular, we describe the SAS3D treatment of fission gas/sodium vapor mixtures and compare it to independent two-fluid models in

the PLUTO2[20,21] and TRANSIT-HYDRO[22,23] codes. Also described are pressure and flow distributions from these refined analyses and an interpretation of their implications on the whole core scenario.

Finally, a few comments should be made about the phenomenology of plenum fission gas release, its potential for fuel compaction, and the conservative modeling of this effect employed in the SAS3D analysis to be described in section III. As discussed in previous meetings with the NRC staff and its consultants, the model used in SAS3D for the compaction is simply an acceleration based on the time dependent pressure difference between the fission gas plenum and the point in the disrupting channel where the non-disrupted pin exists. The mass and length of this accelerating segment decrease as the power burst disrupts additional axial segments and the plenum pressure decreases as gas is ejected into the coolant channel and the gas plenum lengthens because of the downward motion of the accelerating segment. This compactive motion is extremely conservatively modeled by assuming that all fuel pins relocate coherently and all assemblies (typically 12 to 24 asemblies per SAS3D channel) in a given SAS3D channel also respond coherently. Due to significant, radially incoherent, thermal profiles in steady-state and the expected 1 to 2 second time delay in radial void propagation[25], the assumed intra-subassembly coherence must be recognized as a simplifying, conservative assumption. In the TREAT R8 test[11] discussed below, which was designed and executed to explore plenum fission gas effects, such incoherencies required pressurization of only 3 of the 7 pins used. A second mitigating factor not included in the SAS3D analysis is the upward ejection of cladding segments during the expulsion process. In the aforementioned R8 test, it was found that the three pressurized pins upper cladding segments had moved upward from their original locations by 6.4, 10.2, and 74.3 cm, respectively. The smaller

two displacements were for pins which were restricted by the integral instrument sheaths at the tops of these instrumented pins. It would be expected that larger relocations would be more typical of the CRBRP case. Such an effect alters the calculation, and reduces the driving pressure, in two ways. First, the plenum volume increases, thereby reducing the overpressure and, second, the gap length used in the blowdown calculations decreases allowing the plenum pressure to decrease more rapidly. Calculations carried out with no restriction on the upward motion of the plenum gave the result that the plenum moved up far enough (14 in) to reduce the gap length to zero in only 27 ms [See Appendix D]. Clearly, a strong mitigating potential for depressurization is available that has not been included in the present assessment. In addition, the fuel pin motion calculation does not include any friction or mechanical interference between fuel and cladding. Although such restrictive forces are expected to be present, quantification of their effect without experimental guidance is difficult. Consequently, the additional conservatism of ignoring these mitigating forces has been employed in the analysis. In summary, several factors can be identified that mitigate, if not eliminate, the potential for plenum fission gas compaction and the results discussed in the whole core analysis section should be viewed as conservative if such compactive effects play a significant phenomenological role.

II. Phenomenological Considerations

In the previous assessment of the hypothetical unprotected loss-of-flow accident[1], it was concluded that the positive reactivity that could be introduced into the system was sufficiently limited that power levels remained relatively low. The scenario time scale was thus extended and release of the plenum fission gas prior to pin disruption in all SAS3D channels was predicted. It was observed, however, that in the simulation of TREAT LOF tests L6 and L7, and from the test data itself, a slight positive contribution to reactivity from the initial fuel motion could be inferred in relatively low power (5 to 10 times nominal) excursions[8]. This effect was accounted for in the SAS3D/SLUMPY analysis but because the system was sufficiently far from prompt critical, the initial positive fuel effect was of little significance. The maximum reactivity was approximately 60¢. Fuel dispersal in the lead channel mitigated concern for an accelerating sequence in which compactive fuel motion in several more channels made reinforcing positive contributions. In this calculation[1], it is noted, though, that the clad relocation module of SAS3D, CLAZAS[26], was predicting several tens of cents of positive reactivity during this portion of the scenario. As will be demonstrated below, it is believed that CLAZAS overpredicts both the rate and the amount of clad relocation. If similar CLAZAS modeling were used in higher void worth cores, it would predict higher than expected clad reactivities and introduce the potential for nearing prompt criticality at the time of fuel disruption. It should also be noted that the whole core calculations in the previous assessment[1] did not explicitly account for the presence of ejected fission gas in the coolant channel and its effect on the sodium vapor dynamics. The expected local pressurization at the ejection site would reduce the sodium vapor flow in the active core region where the molten cladding is

present and partially remove the shear coupling between vapor and clad, thus mitigating the extent of upward relocation. Such a consequence has been deduced from the TREAT R8 experiment[11]. Although many in-pile experiments have demonstrated the existence of upper cladding blockage, the R8 TREAT test, the only test with substantial pressurized plenum gas release, did not show such an upper blockage.

In this section, we review the important phenomenological areas of the influence of plenum fission gas release on sodium vapor dynamics and clad relocation, dynamic clad relocation under experimental loss-of-flow conditions without fission gas effects, and the failure of irradiated cladding under transient loading by the plenum fission gas. In the first area, we focus on the TREAT R8 experiment and a recent analysis of this experiment with version 1.0 of SAS3D with the modifications and improvements used in the whole core analysis of the CRBRP heterogeneous core. Specific details of flow patterns and comparisons with the experimental data are provided. A parametric study of vapor-cladding frictional drag is presented and compared to experimental information to provide a qualitative basis for the modeling in the whole core analysis. More detailed dynamic information from TREAT and SLSF experiments and their analysis with SAS3D is then reviewed to provide quantitative foundations for the whole core analysis. Finally, experimental information and analytical results are summarized to establish the quantitative clad failure criteria used in the analysis in the third section.

II.1 Modelling of Plenum Gas Blowdown in R8

TREAT experiment R8[11] addressed issues related to voiding dynamics and clad relocation with the presence of released plenum fission gas. In this 7-pin test, 3 of the 7 pins were initially pressurized (4.14 MPa at 560°C) using xenon gas to account for intrasubassembly incoherence. This was a constant, nominal power test subjected to a simulated FFTF flow coastdown. Important observations included the upward ejection of the upper cladding segments, driven by plenum gas expansion, which would have the tendency to mitigate any disrupted fuel compaction. Also observed was that when the cladding subsequently melted, little or no molten cladding was driven upward into the upper reflector region since the channel pressurization had removed sodium and effectively precluded upward sodium vapor streaming at that time. The complete planar blockage at the top of the core found in previous tests was absent in R8, replaced by an inhomogeneous pattern of debris and complete unblocked regions which were the result of the previous cladding ejections. In R8, the remaining cladding melted downward faster than in previous tests, due to the early, complete channel voiding. The channel pressurization due to plenum gas release resulted in the predicted expulsion of sodium from the entire core region; this early voiding and ensuing film dryout altered the subsequent heatup, melting, and relocation of cladding relative to previous tests. A complete inlet blockage formed about 2 s earlier in R8 than in previous tests, attributable to the much hastened downward melting progression in the absence of sodium "chugging". The blockage lower extremity was 8 cm into the lower reflector region; by the end of the test the steel had accumulated to 21 cm thickness.

The R8 test was re-analyzed using the new SAS3D treatment of fission

gas/sodium vapor mixtures as well as a minor code modification, described in Appendix C, to account for the system hydraulics. The main purpose of this re-analysis was to determine whether the CLAZAS model, using coolant velocities and pressures calculated by the new gas/sodium vapor treatment, could predict the clad relocation results observed in this test. It was found that CLAZAS could predict the observed clad relocation results, but only if the friction factor used to calculate the shear stress between the sodium vapor and molten clad were reduced to a nominal single phase friction factor, rather than the flooded two-phase friction factor normally used in CLAZAS.

For this re-analysis of R8, a number of SAS3D input parameters were different from those used in the SAS analysis reported in ANL/RAS 78-39[11]. The pin failure was assumed to occur in an axial node centered 12.8 cm below the top of the active fuel, since SAS3D predicted the highest clad temperatures at this node at the time of pin failure. At the time of clad failure, SAS3D predicts that the gap between fuel and clad at the top of the active core is smaller than the gap between the upper Inconel reflector and the clad. Therefore, the flow area and hydraulic diameter of the flow path between the gas plenum and the rupture were based on the calculated gap size between fuel and clad in the upper active fuel nodes at the time of pin failure. The length used for this flow path was 18 cm, which corresponds to the length of active core above the assumed failure point plus a small addition for the pressure drop past the upper Inconel reflector. As shown in Figure 1, with the use of these parameters, SAS3D predictions for the plenum gas blowdown agree quite well with the experimentally observed results.

Table 2 gives the timing of many significant events in this test. For the SAS3D calculations, a cladding failure temperature of 1400°C was used. Near the time of clad failure, the clad temperature at the failure

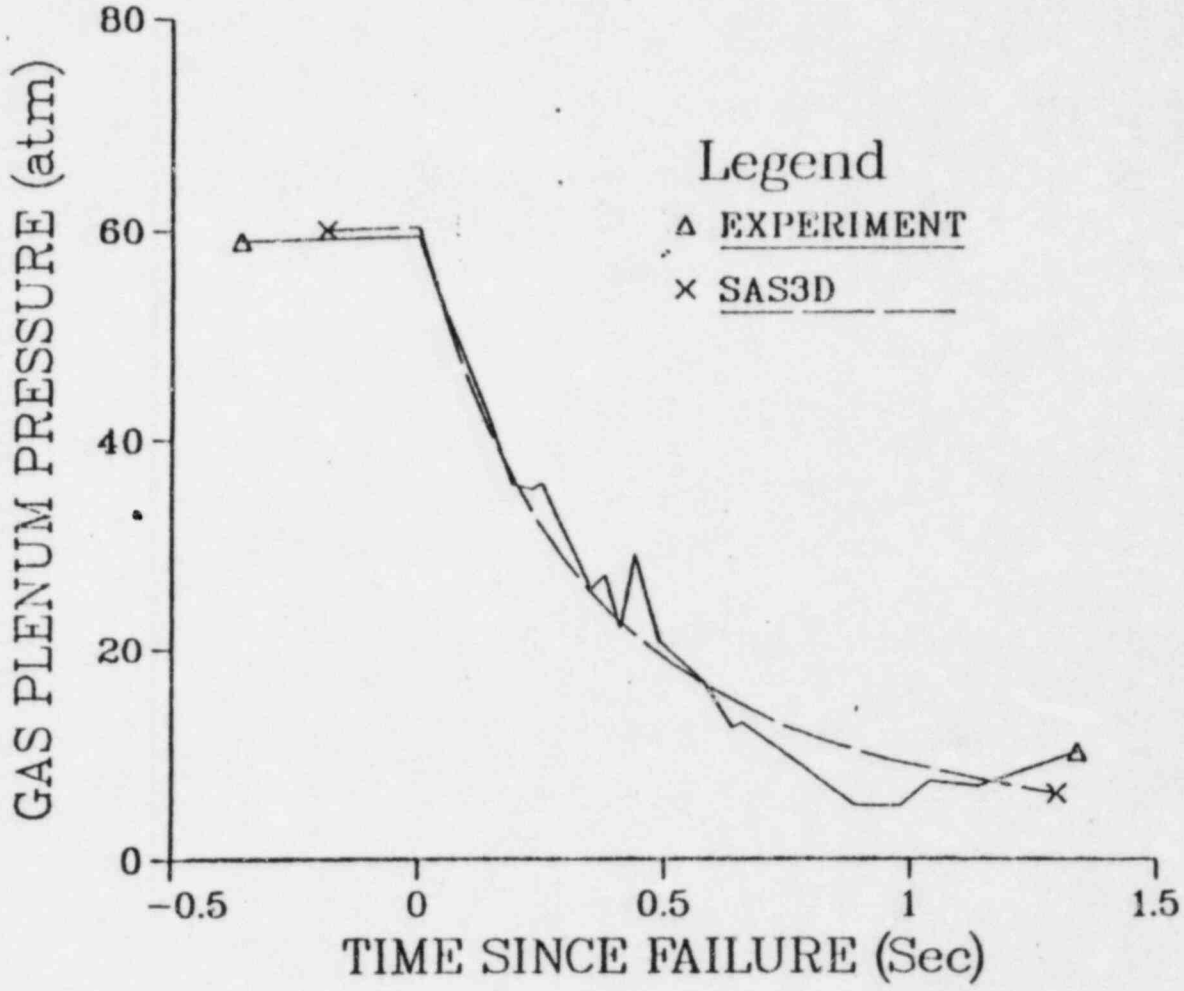

Figure 1. R8 Gas Plenum Blowdown

Table 2. Timing of Events in the R8 Test

Event	Experiment Time (sec)	SAS3D Time (sec)
Reactor power up	3.5	3.5
Start of flow coastdown	7.97	7.97
Local boiling	15.17	-
Net voiding	17.5	17.52
Inlet flow reversal	18.18	18.17
Onset of cladding failures	18.89	18.93
Flowtube failure	18.96	-
Cladding motion starts	-	19.42
Reactor power down	26.0	26.0

node was increasing at a rate of about 700°C/second, so the SAS3D failure time would match the experimental value better if a clad failure temperature of about 1370°C were used. Since unirradiated clad was used in this test, the clad failure temperatures in the test were probably higher than they would be for end-of-life irradiated clad.

Figure 2 gives a comparison of the measured and computed inlet flow rates for R8. The agreement is reasonably good from the beginning of the run through the initial boiling, the clad failure, and the initial expulsion and re-entry after gas release starts. Later, when SAS3D predicts the re-entry of liquid sodium over very hot clad, the code predicts some vigorous expulsion and re-entry events with higher frequencies and higher amplitudes than those observed in the experiment. The SAS3D calculation shown in Figure 2 used the normal CLAZAS two-phase flooding friction factor for the shear stress between sodium vapor and molten clad. Figure 3 shows the results obtained when the same case was re-run with a nominal single phase friction factor in CLAZAS

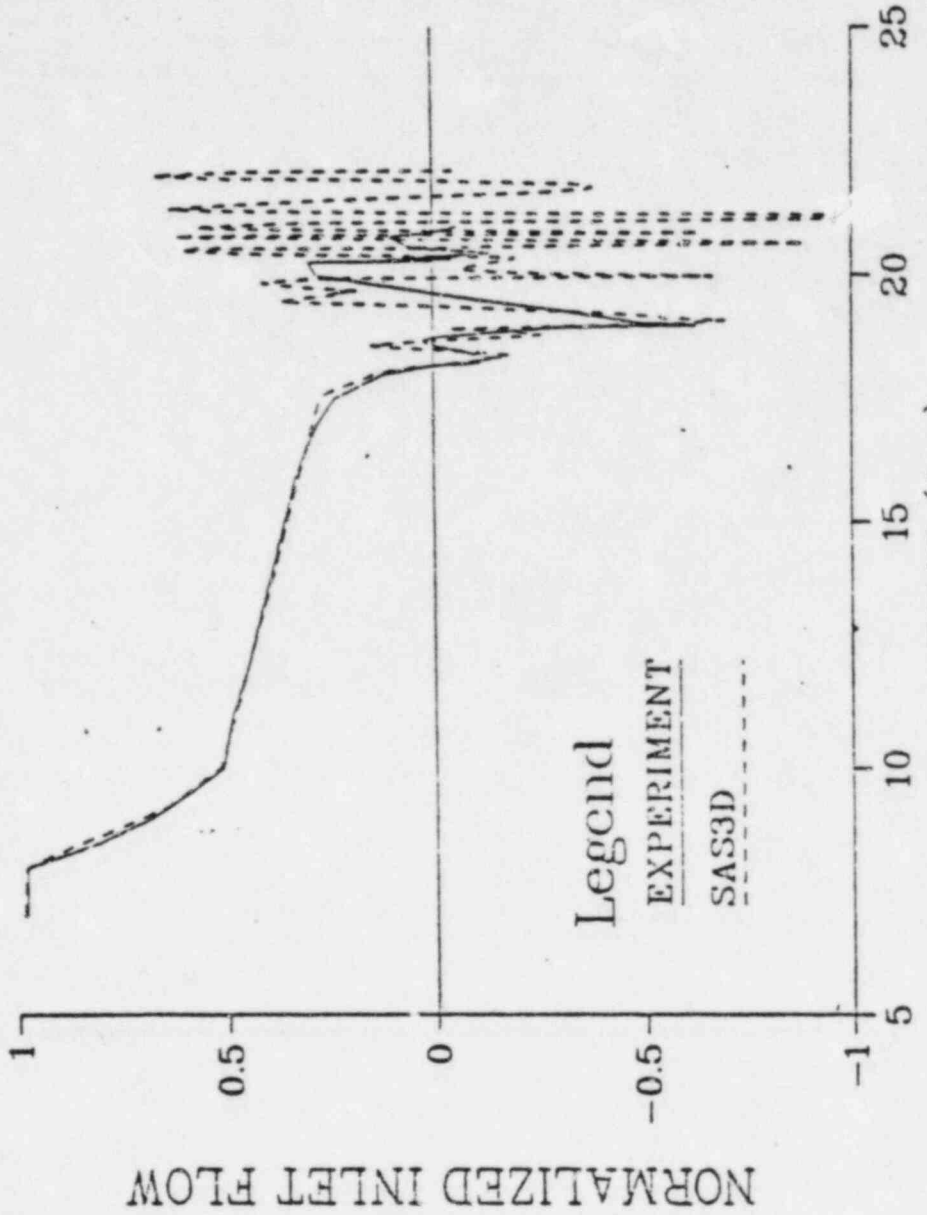

Figure 2. RB Coolant Flow Rates, Flooded Friction Factor in CLAZAS

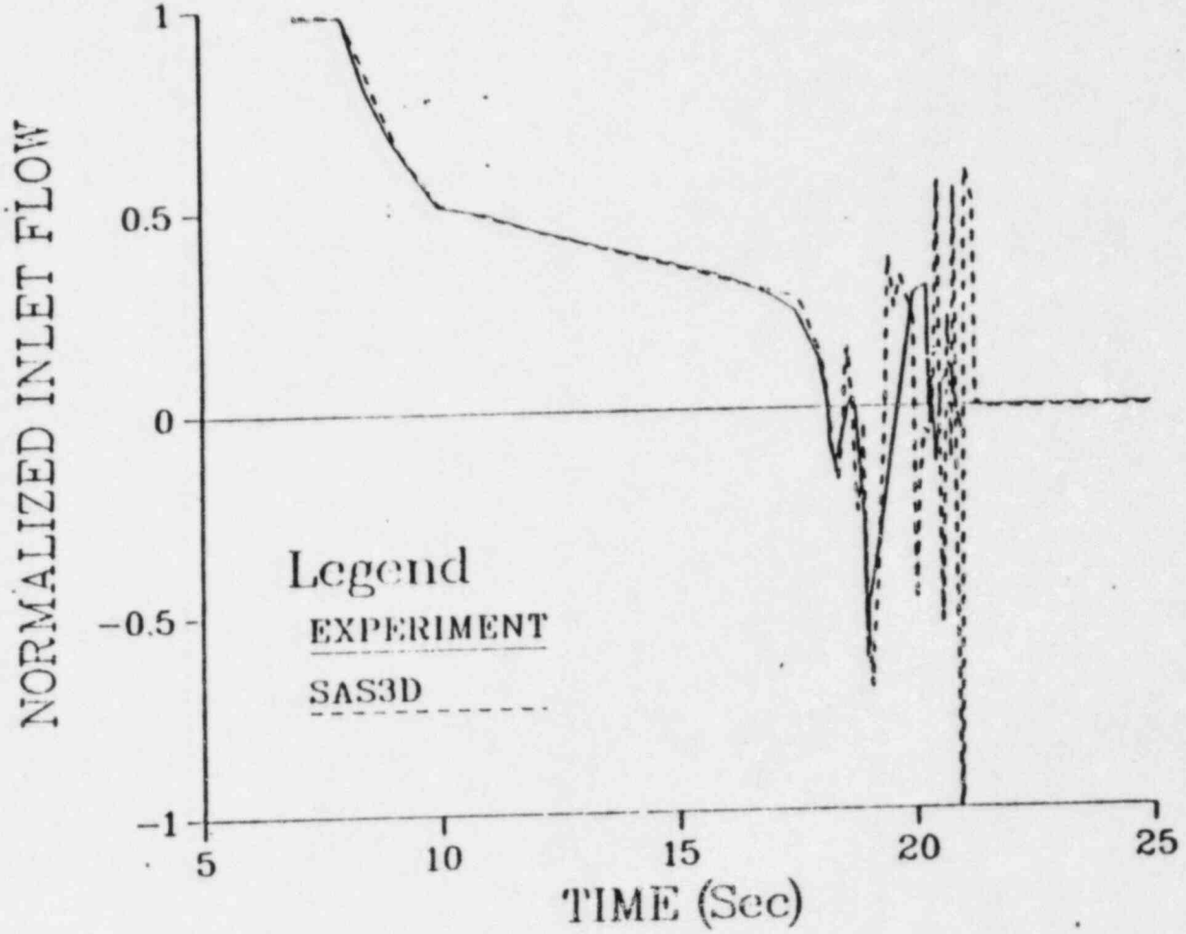

Figure 3. R8 Coolant Flow Rates, Nominal Single Phase Friction Factor in CLAZAS

instead of a two-phase friction factor. Until the start of clad motion, both cases are the same, but after clad motion starts the nominal single phase case quickly predicts a clad blockage in the lower part of the active core, and this blockage reduces the amplitude of the liquid sodium re-entry and expulsion. Flowtube failure which occurred soon after the start of gas release from ruptured pins was not modelled in SAS3D, but it would probably have some impact on coolant flow rates. Another aspect that was not included in the SAS3D analysis was the upward ejection of the upper clad segments of the pressurized pins after pin failure. The upper parts of two pins restricted by instrument sheaths went upward 6.4 and 10.2 cm, whereas the upper clad from the third pin went upward 74.3 cm. If the upward motion of the clad from the third pin occurred soon after pin failure, it would have led to very rapid gas release from that pin, although the ejection of the upper clad segment would have reduced the impedance to upward flow for gas from the pin, and thereby would have reduced the impact of the rapid gas release on the inlet flow shown in Figures 2 and 3. The measured gas pressure shown in Figure 1 is for the pin that moved upward 10.2 cm. An upward motion of 10.2 cm would reduce, but not eliminate, the impedance to gas flow between the gas plenum and the rupture point. It is possible that the impedance in this pin was initially higher than that modelled in SAS3D, and that the impedance dropped as the upper clad segment moved upward.

The expulsion of the inlet liquid after pin failure was somewhat faster in the SAS3D results than the experimental measurements indicate, and SAS3D predicts re-entry after the expulsion sooner than the experiment. In the SAS3D analysis, all three pressurized pins were assumed to fail simultaneously. Staggering the pin failures would reduce the speed of the initial expulsion and delay the re-entry.

At 19.42 seconds, when the motion of molten clad starts, much of the gas has been released from the gas plenum; but the plenum gas pressure is still 19 atmospheres at this time; and gas release still has a large influence on the pressures and flow rates in the coolant channel. Figures 4 and 5 show the coolant pressures and mass fluxes near the time when clad motion starts. The gas is being released at 98 cm. The pressure peaks at this location. The mass flux is upward above this location, and downward below it. If the gas were not being released, then by the time that clad motion starts the coolant pressure would tend to peak near the bottom of the active core, where the vapor source would be, and the vapor velocities would tend to be upward above that point.

After the start of clad motion, gravity and downward gas flow tend to send the clad downward, but periodic re-entry of liquid sodium into the bottom of the fuelled region provides an intermittent vapor source that exceeds the gas source and sends vapor and clad upward part of the time. Figure 6 shows the coolant pressure profile soon after a re-entry. Re-wetting of hot clad provides a high vapor pressure near the bottom of the fuel. Molten clad causes partial blockages at several axial locations. Most of the pressure drop in the test section is concentrated across these molten clad regions, and the combination of pressure gradients plus shear stress from upward streaming vapor sends clad upward when the hot clad is wetted.

Figure 7 shows the clad behavior for the case with a flooded friction factor between clad and vapor. In this figure, shaded areas represent molten or re-frozen clad, and the density of the shading is an indication of the thickness of the clad. The clad oscillates up and down, but eventually a substantial clad blockage is formed above the core and the rest of the clad drains downward. Even with a substantial gas source near the top of the fuel,

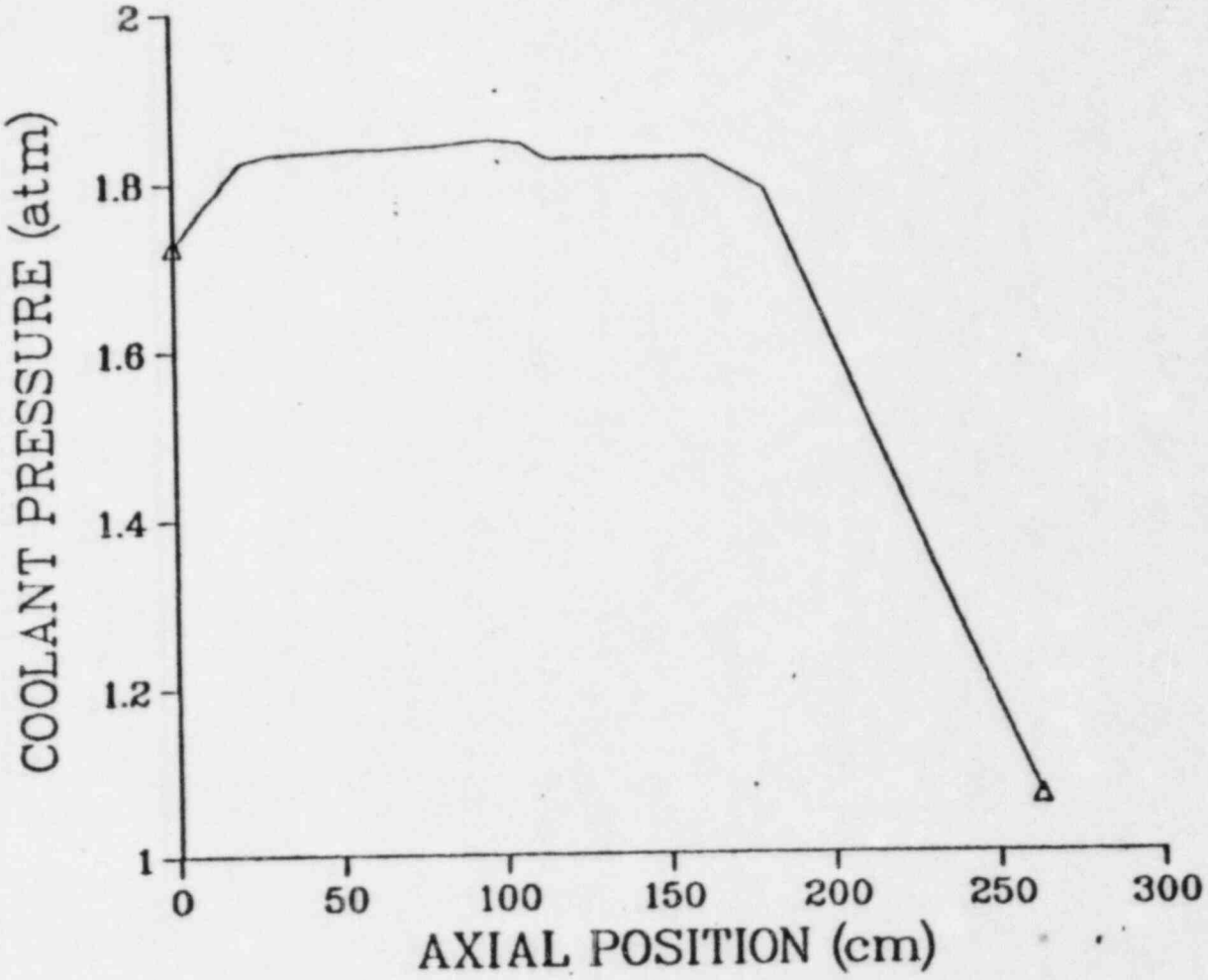

Figure 4. Coolant Pressure Profile at the Onset of Clad Motion

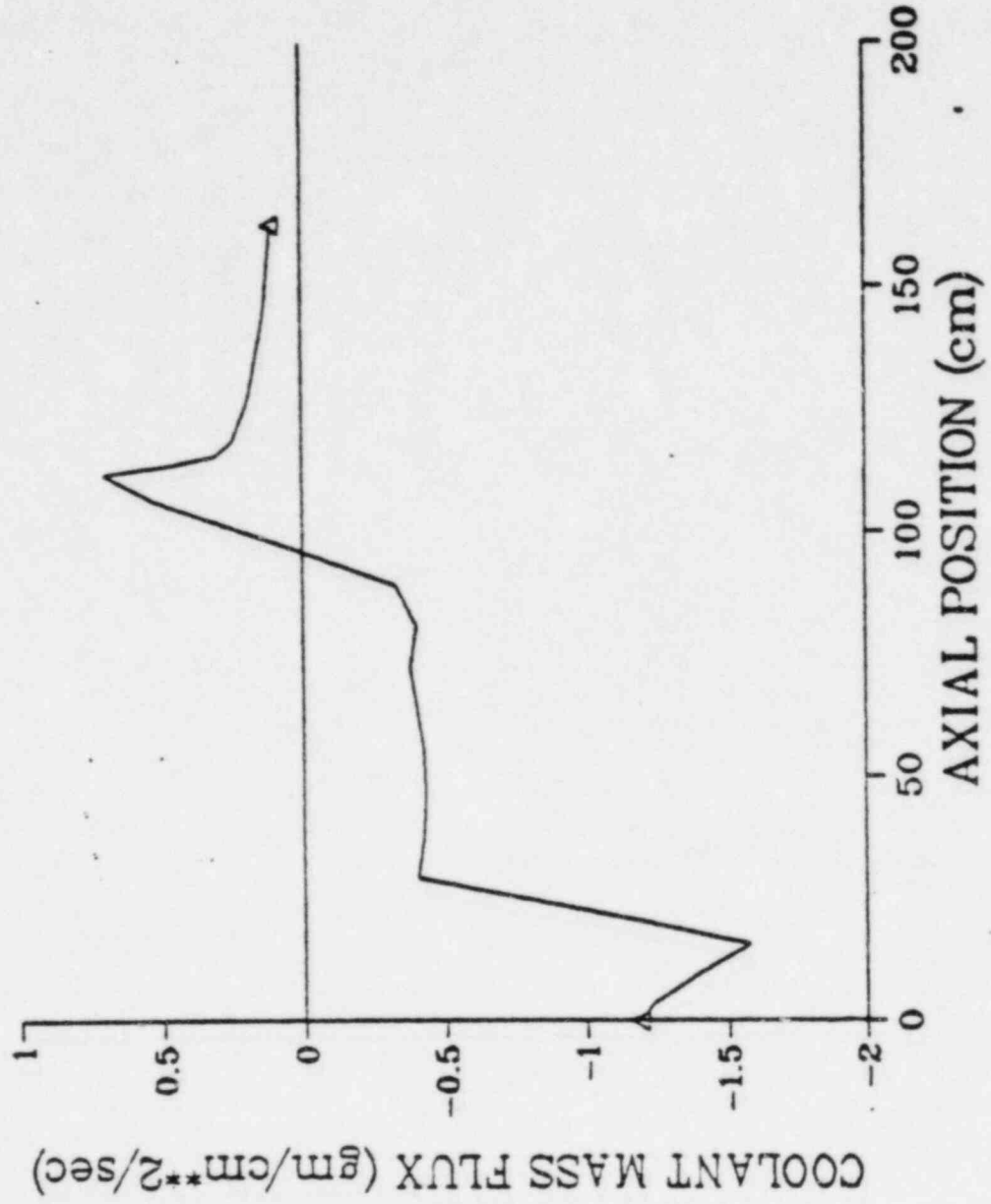

Figure 5. Vapor Mass Flux at the Onset of Clad Motion

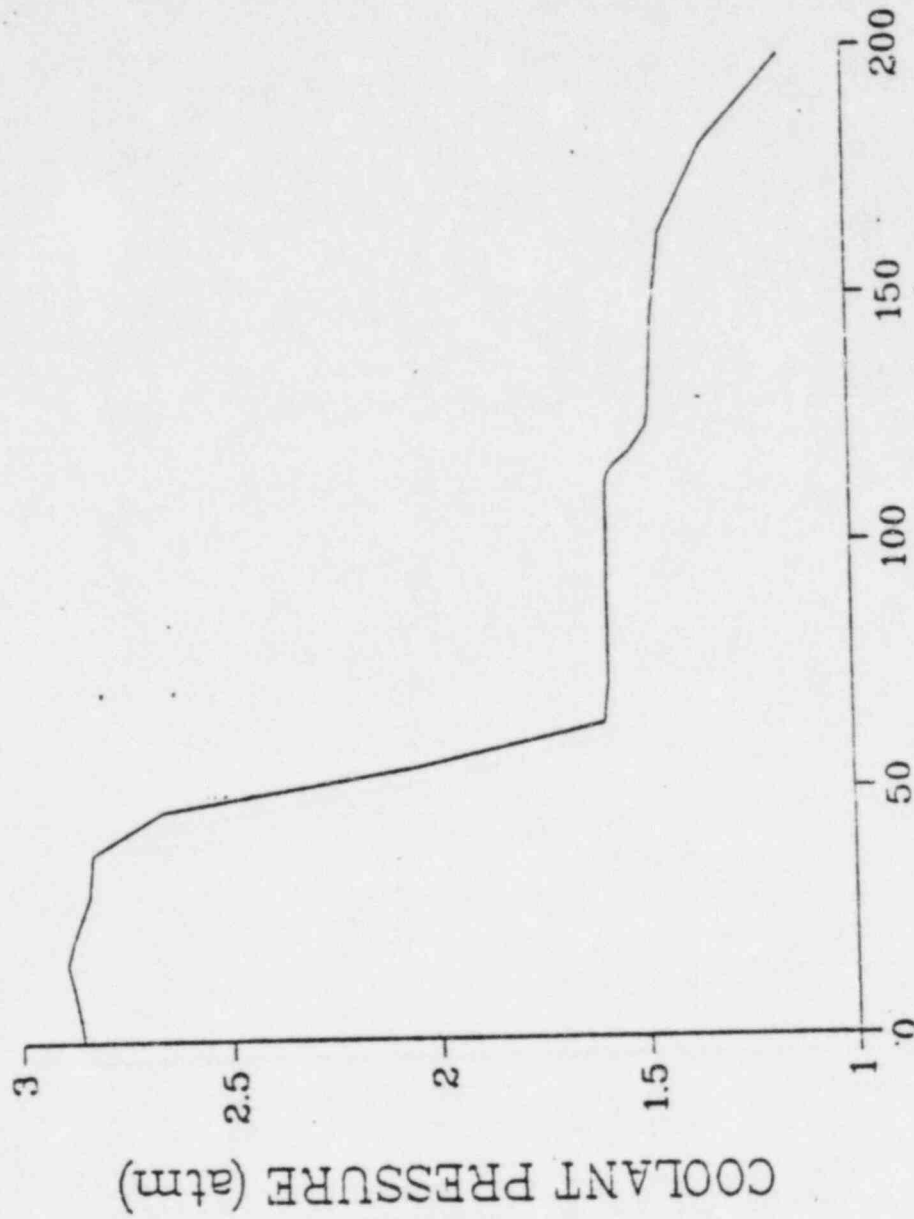

Figure 6. Coolant Pressure Profile After a Re-entry Event

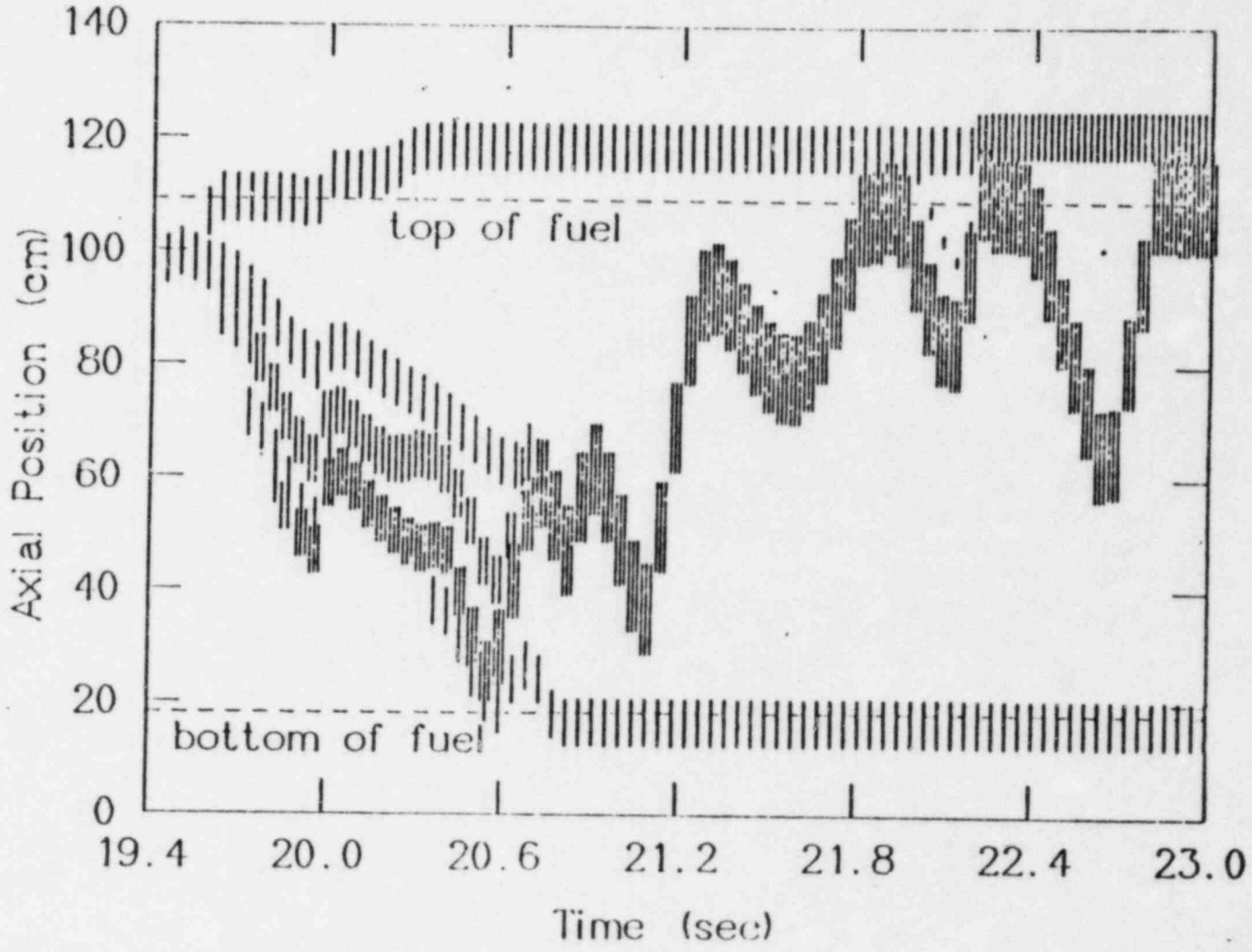

Figure 7. R8 Clad Motion, Flooded Friction Factor in CLAZAS

much of the clad goes upward. A post-test examination of the test section showed no clad blockage above the core, and no indication that molten clad had ever gone upward into the reflector region. Instead, all of the clad from the fuelled region was found in a massive blockage in the lower reflector. Figure 8 shows the results of the same case re-run with a nominal single phase friction factor between the sodium vapor and molten clad. In this case, all of the clad ends up in the lower reflector. In either case, the coolant pressure gradients tend to concentrate across the molten clad regions, but the difference in shear stress is enough to make the difference between net upward motion and net downward motion.

In summary, the use of a flooded friction factor in CLAZAS over-predicts the upward motion of molten clad in this test, whereas the results calculated with a nominal single phase friction factor are consistent with the post-test examination. Also, the nominal single phase results provide better agreement with the measured inlet flow after the onset of clad motion.

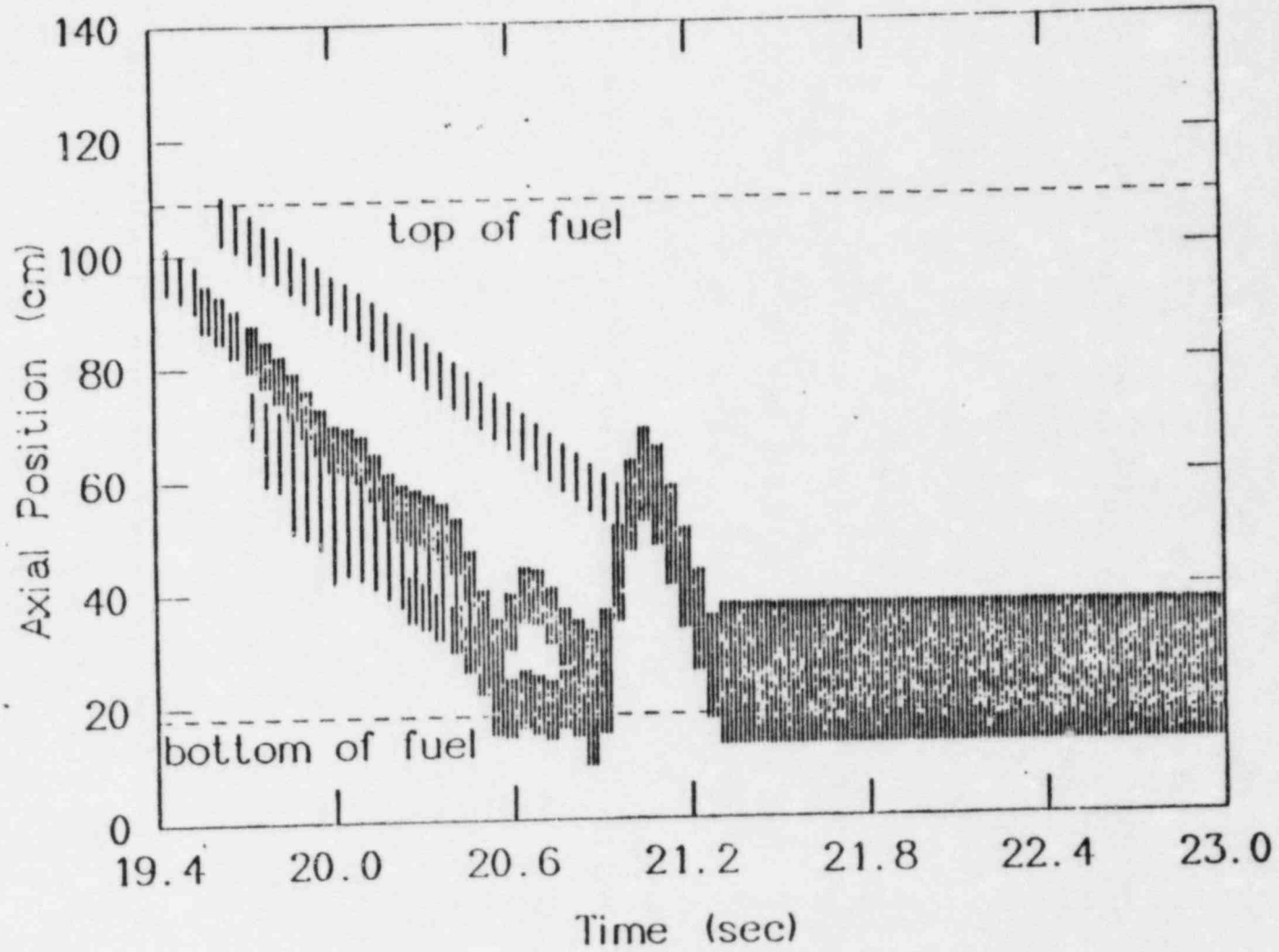

Figure 8. R8 Clad Motion, Nominal Single Phase Friction Factor in CLAZAS

II.2 Experimental Results on Clad Relocation Dynamics

To assess further expected clad relocation in the CRBRP LOF scenario, several additional experiments and their analyses with the SAS3D code, were reviewed to establish a reasonable treatment within the context of the SAS3D code. The experiments considered were the TREAT R4 and R5[10] tests, and SLSF tests P3[13] and P3A[12]. SAS3D analyses of these tests have been performed as well as analyses with the one dimensional cladding relocation model, CLAP[27], for the R5 test and the multi-dimensional cladding relocation model, MULCLAD[28,29], for the R4, R5, P3 and P3A tests. A brief summary of the tests, their results, and the analyses is provided below.

TREAT tests R4 and R5 were seven-pin, loss-of-flow tests with full-length unirradiated FFTF-type fuel pins. In LOF test R4, the sequence was run at constant, nominal power well beyond the inception of molten fuel motion. In R5, the sequence was terminated prior to fuel melting to preserve evidence of early molten cladding motion. Up to the point of fuel melting and motion, the tests were consistent with each other. It was noted, however, that the thermocouple data for the R4 test were of good quality, but the R5 data showed numerous ambiguities attributable to erratic thermocouple performance. Consequently, the interpretation of temperature data was based principally on R4 data. It was noted in reference 10 that: "..., at a time in the test sequence when SAS calculates the onset of cladding motion (about 1 sec after the cladding solidus temperature is reached), thermocouple TCTS-7, located 3 inches below the top of the fuel column, indicates a rapid transient heating event. This is interpreted as being caused by the motion of molten cladding material which accumulates and bridges to the flowtube wall. Additionally, thermocouple TCTS-5, at the top plane of the fuel column, shows a similar heating event about 0.1 sec after the lower TC, suggesting a net upward motion

of the molten material. However, thermocouple TCTS-4, located one inch above the heated zone in the colder insulator pellet region, does not show such an event, suggesting that the molten material stopped its upward motion between these two measurement locations". This upward relocation of 3 to 4 inches in 0.1 sec implies an average upward cladding velocity of less than 100 cm/sec. The presence of the upper cladding blockage was confirmed during post test examination and were found to be about 0.3 cm in thickness.

A post-test analysis of the R5 test was performed with SAS3A code and summarized in reference 10. To examine the effect of the frictional coupling between streaming sodium vapor and molten cladding, this same experiment model was examined with version 1.0 of SAS3D[30] with the modifications described in the appendices. The most important modification was the consistent coupling of frictional effects in the "flooded" cladding region[26] with the implication of reduced vapor flow and reduced shear forces on the molten cladding. Figure 9 shows a comparison of inlet flow rate between SAS3D and the experimental measurements and the results are seen to be quite good. SAS3D predicts the initiation of clad motion in node 15, whose mid-point is at 97.5 cm from the bottom of the pin (11 cm below the top of the active fuel). As mentioned earlier, it was reported that a thermocouple 3 inches below the top of the active fuel sensed molten clad motion initially and a second thermocouple at the top of the fuel sensed molten clad motion approximately 0.1 sec later, implying a clad velocity of approximately 75 cm/sec. In SAS3D calculations with the normal flooded two-phase friction factor, initial velocities were calculated in excess of 200 cm/sec and in the time it took the clad to move 10 cm, the average velocity was approximately 150 cm/sec. By reducing the frictional coupling by employing a nominal single phase friction factor[26], the initial velocities were calculated in the range of 50 cm/sec and in the time

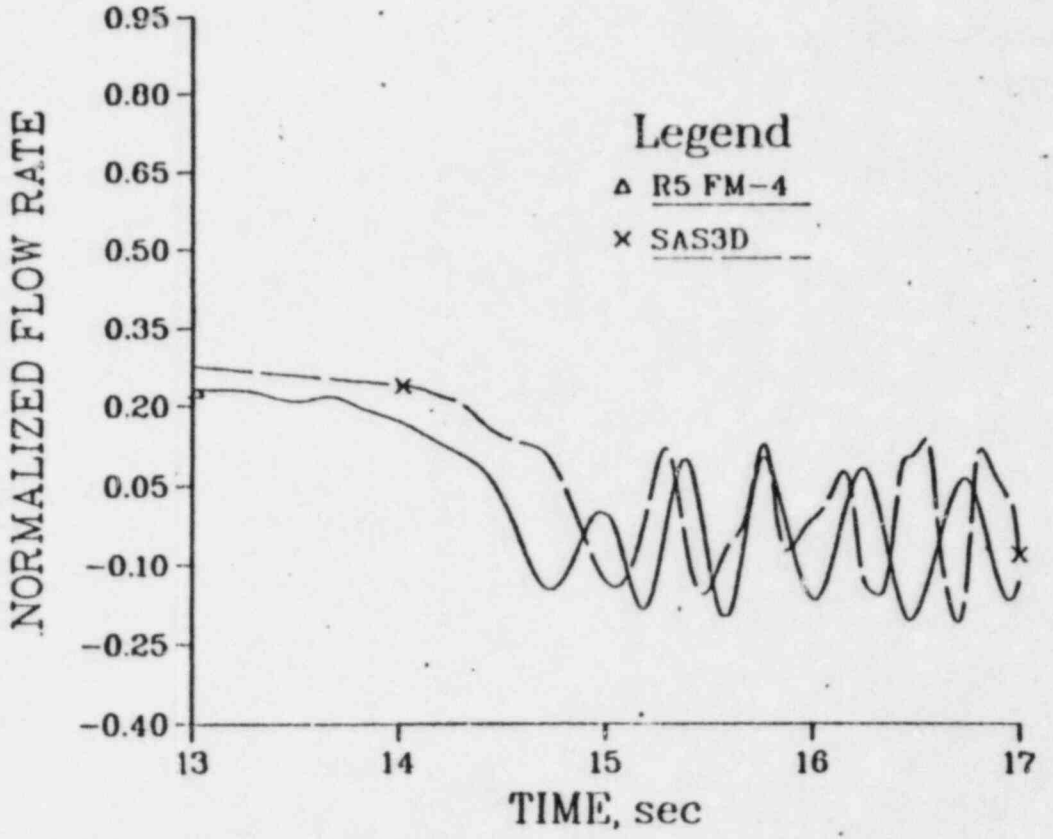

Figure 9. R5 Inlet Flow-rate Comparison

it took the clad to move 10 cm, the average velocity was approximately 75 cm/sec. Recognizing that there is uncertainty in the experimental measurements, it is still clear that the modification of frictional coupling to using a nominal single phase friction factor has resulted in a reduction in the rate of upward clad relocation and provides better agreement with the experimental data. In the review of a similar event sequence and calculation from the P3A experiment and the qualitative results for clad motion in the R8 experiment, it will be seen that such a reduction in upward driving forces is consistently required to reach reasonable agreement between SAS3D/CLAZAS calculations and experimental observations.

Such apparent deficiencies of CLAZAS have long been recognized, however, and a new cladding relocation model, CLAP[27], was, in fact, developed several years ago and incorporated in the SAS3A code. In the analysis of the TREAT R5 test with CLAP, it was noted "In comparison to CLAZAS calculations of the type of experiment, the CLAP model allows calculation of a more realistic smaller upper blockage,...".[27]

Analyses of TREAT experiments illustrate that clad relocation predictions with SAS3D/CLAZAS should be viewed with caution. Similar conclusions were drawn from the SLSF P3A and P3 experiments and their analyses. The P3A experiment contained a fuel bundle comprising 37 fresh, full-length, prototypic FTR pins. The fuel was irradiated in the SLSF under prototypic thermal conditions to an equivalent of 26 full-power days, at maximum average linear power of 36.7 kW/m, yielding a maximum burnup of ~0.6 atom %. Following 48 hours of continuous full-power operation, the fuel was subjected to a simulated loss-of-flow accident. The test train orificing and bypass flow had been chosen such that the boiling and voiding dynamics that resulted from the flow reduction closely approximated those expected in a loop-type fast

reactor. Thus, the test produced data on voiding and cladding motion, as well as data on fuel disruption characteristics.

This experiment and the SLSF experiment P3, which used a nearly identical test vehicle and test conditions, form a complementary set of experiments addressing the behavior of low-burnup fuel bundle during an LOF. The reactor scram in the P3A LOF simulation was chosen to terminate the experiment just before gross fuel melting, and thus to yield data on initial fuel disruption. The P3 LOF simulation was continued long enough to ensure widespread fuel melting and to provide an opportunity for early fuel motion.

The prediction of coolant voiding by SAS3D was observed to be reasonably good, but the clad relocation sequence, as deduced from thermocouple response, developed more slowly than that predicted by the code. Specifically, a thermocouple positioned 76 mm below the top of the fuel detected molten steel at 12.2 sec and a second thermocouple positioned at the top of the fuel, rose to the stainless steel melting temperature between 12.5 s and 13.0 s in the P3A test. The timing of cladding events and comparisons with calculations are given in Table 3 [taken from Reference 12]. In the SAS3D/CLAZAS analysis of this experiment reported in reference 12, the initial clad velocities were calculated to be greater than 200 cm/sec and over the first 0.1 sec, they averaged sightly less than 200 cm/sec. In this analysis, the normal flooded two-phase friction factor was used. Measured clad motion is seen to be less than that predicted by SAS3D/CLAZAS, with average velocities in the 20 to 30 cm/sec range. Similar results were obtained in comparison of experimental results and analyses for the P3 test.

Table 3[12]

Timing of Cladding Events in P3A Experiment
(times in seconds after beginning of coastdown)

	SAS3D	P3A DATA
Initial Cladding Melting	10.3	11.8
Initial Cladding Meltthrough and Motion	11.0	11.8-11.9
Molten Cladding Reaches Top of Fuel	11.1	12.5
Top Blockage Reaches Final Configuration	11.1	~13.0
Configuration of Top Blockage	Complete	Partial
Bottom Blockage Complete	11.6	NA

The tests discussed above have illustrated that the CLAZAS module of SAS3D can qualitatively predict the behavior of molten clad relocation including the development of upper blockages and the subsequent draining to form a lower blockage. There are limitations, however, in the quantitative predictions of rates of relocation and the extent of the upper blockage.

From the review of these experiments and the R8 analysis in the previous section, it is clear that modeling clad relocation with the one-dimensional CLAZAS module of SAS3D using the high frictional coupling appropriate for "flooded" conditions can produce conclusions that are both qualitatively as well as quantitatively incorrect. Consequently,in the whole core cases to be described in section III, using the fact that CLAZAS clad relocation predictions were more consistent with experiments with significantly weaker vapor-clad frictional coupling, the choice of a nominal single phase friction factor was employed.

II.3 Cladding Failure Criteria

In our previous SAS3D assessment of the potential for autocatalysis due to plenum pressure driven fuel compaction[1], we made the simplifying assumption that blowdown of the plenum would not begin until the cladding at the top of the active fuel reached 1400°C; essentially the melting point. Although the cladding at the fuel-blanket interface will certainly fail by the time it reaches melting, earlier mechanical failure must occur at some temperature less than melting under EOC-4 plenum pressure loadings of the order of 50 atmospheres. Earlier failure would allow more time for depressurization. For typical cladding heating rates near melting of 100-500°C/s, a reduction in the failure temperature of 100°C would increase the blowdown time by 0.2-1.0 seconds. This additional time is substantial compared to the time constant for blowdown of about 0.25 s [See Appendix D]. We have therefore looked more carefully here at the question of cladding failure under plenum pressure loading.

Cladding failure temperatures depend on steady state irradiation history, mechanical loading, and transient thermal history. Table 4 provides the most important parameters as determined for the uppermost active fuel column cladding node from the new best estimate case SAS3D calculations of the CRBR EOC-4 loss-of-flow accident scenario (Case 1 in section III). The channel numbers at the top of the table refer to SAS channels as given in Reference 2. The cladding hoop stress σ is calculated from the maximum plenum pressure P and the thin shell formula $\sigma = Pr/h$, where r is the inner cladding radius and h is the cladding wall thickness. Also shown are the cladding midwall heating rates at temperatures near the melting point.

Our reassessment of cladding failure under the conditions given in Table 4 consisted of a review of relevant experiments plus calculations using both

Table 4

Heating Rates for SAS3D Best Estimate LOF Case

	CH 2	CH 4	CH 6	CH 7	CH 11
Fluence at Top Node 10^{22} n/cm^2	6.34	6.37	3.44	6.98	7.56
Irradiation Temperature, °C	572	569	587	564	555
Maximum Plenum Pressure, MPa	4.4	4.4	2.3	4.4	4.4
Cladding Hoop Stress at Maximum Plenum Pressure, MPa	29	29	15	29	29
$\dot{T}$ @ 1200°C, °C/S	225	219	154	208	526
$\dot{T}$ @ 1300°C, °C/S	216	246	141	365	443
$\dot{T}$ @ 1400°C, °C/S	347	432	166	433	320

data correlations and theoretical models. The experiments which we judged to be most directly applicable to the question of cladding failure under plenum gas loading conditions were the FCTT tests performed at HEDL[14-17]. In the FCTT tests, both unirradiated and irradiated cladding tubes were internally loaded with gas pressure and heated uniformly at a constant rate until failure occurred. Failure temperature and failure ductility were measured as a function of heating rate and initial hoop stress. These tests very closely simulate the thermal and mechanical loading conditions of interest here. Furthermore, multiple FCTT tests[18] have shown that the most important part of the

cladding thermal history is that part near the failure temperature. For low pressures, where failure is expected to occur near the melting point, Table 4 shows that the SAS3D calculated cladding heating rates at the fuel blanket interface are nearly constant and of the order of several hundred °C/s. Such heating rates are close to the highest heating rate (111 °C/s) FCTT data. Some additional data does exist from recent FCTT TUCOP[19] tests at higher heating rates of 550°C/s. However, in the TUCOP tests the cladding diametral strain-rate was controlled by decreasing the driving pressure as the test proceeded. Since plastic instability is an important aspect of high-temperature failure under constant pressure loading, these tests tend to give somewhat higher failure temperatures than would be expected under constant pressure conditions.

Although a considerable amount of FCTT data exists, almost all of the data are for conditions where the gas pressure loading was greater than 50 atmospheres. We have to make use of the full data base here to calculate failure under low-pressure conditions by extrapolating existing correlations[16,33] of the data. In our calculations, the Dorn parameter correlation[33] produced the most reasonable results when compared with the limited high-temperature, low-pressure data. Application of the Dorn parameter correlation to the conditions given in Table 4 produced cladding failure temperatures between 1250 and 1300°C.

Additional calculations of cladding failure were performed using theoretical models developed by ANL/RAS[34,35,36]. These models describe the fundamental phenomena which govern cladding failure, including high- and low-temperature matrix deformation, annealing and recovery, grain growth, liquid metal and irradiation embrittlement, and intergranular fracture. Previous comparisons between the theoretical models and the FCTT data mentioned above

have shown good agreement. Extension of these calculations to the conditions given in Table 4 produced failure temperatures for irradiated cladding in the range of 1250-1350°C. It was also found that for unirradiated cladding under similar conditions, the failure temperatures are within 25°C of melting. This result is consistent with the SAS3D interpretation of the R8 TREAT test given elsewhere in this response.

Based on the above review of the relevant data and on calculations using two independent approaches, we conclude that 1300°C is an appropriate average cladding failure temperature to be used to initiate plenum blowdown in the SAS3D assessment of plenum pressure driven fuel compaction in CRBR EOC-4 loss-of-flow accident scenario. This temperature is 100°C less than the previous conservative assumption of cladding failure at melting.

III. EOC-4 LOF Summary

A best estimate LOF scenario for the CRBRP EOC-4 heterogeneous core, incorporating the phenomenological considerations discussed above, will now be described. The basic reactor model is the same 15 channel model used in Reference 2. The neutronics data are the new values which resulted from the reassessment of the sodium void worth described in the introduction. Thus, all the neutronics data are different from those used in Reference 2. Most importantly, in the driver subassemblies, the void worth is somewhat more than 34 cents larger and the steel worths are increased by about 85 cents. Other modeling assumptions, with a few exceptions to be described below, are the same as were used in the response to question CS760.178A3.

Unlike previous whole core calculations using SAS3D[1,2], the current calculation explicitly accounts for the release of stored fission gas from the fission gas plenum into the SAS channel. The manner in which this is accomplished is similar to that used in the analysis of the R8 experiment described above. Coding changes were also introduced to allow (at the user's discretion) the pressure in the fission gas plenum to be applied to the top of the upper pin stub in the SLUMPY calculation. When this option is used, the mass of the upper axial blanket fuel pellets is added to the pin stub mass in determining the downward acceleration of the stub. In addition, coding changes were made to allow the use of smooth-tube friction coupling between clad motion and the sodium vapor streaming. This appears to allow the one-dimensional modeling in SAS3D/CLAZAS to better approximate experimental results. The analysis of the R8 test supports this approach. Clad motion was allowed to begin when the clad melt-fraction reached unity. The boiling model was modified so that after the onset of clad motion the friction factor used to calculate the shear stress between the vapor and the clad in the boiling

model was the same as that used in CLAZAS. Previously, the friction factor used in the boiling model did not account for any flooding that CLAZAS might be using. Finally, code changes were introduced to prevent moving cladding within the SLUMPY compressible zone from causing a zero-velocity boundary condition to be set at one or both edges of the compressible region.

An event sequence for the current calculation is listed in Table 5. This case is designated as Case 1. It is of particular interest to note the times when gas release begins and ends in a channel. The gas release is stopped when the pressure in the fission gas plenum drops below 2.5 atm. This value was typical of the pressures predicted by SLUMPY at the point of fuel disruption in the previous assessment[1]. The time required to achieve this value is seen to vary from as little as about 0.7 s to more than 1.5 s. In addition, it is noted that of all the channels to initiate fuel motion during the transient, only channel 11 does so before the gas release has stopped. In this channel, the pressure in the fission gas plenum is about 4.3 atm when fuel motion initiates, while coolant channel pressures are nearly as high at the axial location where fuel motion begins. Thus, compactive fuel motion is minimal and the potential for autocatalysis is quite small.

It should be noted that in the present calculation, the pressure in the fission gas plenum is held artificially high because of a peculiarity in the gas release model. The pressure used by the gas release model at the clad rupture point is not the coolant channel pressure in the axial node containing the rupture location, but is the pressure at the lower bubble interface for the vapor bubble adjacent to the rupture. Normally, the difference between these two pressures is small enough to have an unimportant effect on the rate of gas release; however, in the present case, the lower bubble interface for channel 11 is located below a molten clad blockage. Because the lower sodium

Table 5
Event sequence for Case 1

TIME	EVENT	CHN*	P/PO	RHO	RHOP	RHOD	RHOE	RHOV	RHOF	RHOC
11.9251	COOLANT BOILING	6	0.863	-0.074	0.0	-0.151	-0.058	0.134	0.0	0.0
13.4879	COOLANT BOILING	2	0.902	-0.013	0.0	-0.172	-0.068	0.227	0.0	0.0
13.8538	COOLANT BOILING	4	0.866	-0.059	0.0	-0.180	-0.073	0.193	0.0	0.0
14.3099	COOLANT BOILING	7	0.880	-0.038	0.0	-0.187	-0.079	0.228	0.0	0.0
15.0174	RELEASE GAS	6	0.987	0.062	0.0	-0.211	-0.098	0.371	0.0	0.0
15.6666	CLAD MOTION	6	1.674	0.394	0.0	-0.270	-0.150	0.814	0.0	0.0
15.7166	STOP RELEASE	6	1.625	0.367	0.0	-0.277	-0.156	0.797	0.0	0.004
15.8066	COOLANT BOILING	10	1.652	0.367	0.0	-0.289	-0.166	0.830	0.0	-0.008
15.8266	COOLANT BOILING	11	1.695	0.381	0.0	-0.291	-0.169	0.853	0.0	-0.012
16.0265	COOLANT BOILING	9	1.706	0.356	0.0	-0.319	-0.194	0.919	0.0	-0.050
16.3609	COOLANT BOILING	13	1.779	0.365	0.0	-0.351	-0.225	0.969	0.0	-0.029
16.3659	RELEASE GAS	2	1.782	0.365	0.0	-0.351	-0.226	0.970	0.0	-0.028
16.5409	RELEASE GAS	4	2.672	0.561	0.0	-0.377	-0.248	1.157	0.0	0.030
16.7656	COOLANT BOILING	12	5.124	0.714	0.0	-0.474	-0.317	1.283	0.0	0.223
16.8109	RELEASE GAS	7	7.089	0.782	0.0	-0.498	-0.336	1.393	0.0	0.222
16.8784	FUEL MOTION	6	8.374	0.790	0.0	-0.549	-0.376	1.489	0.0	0.225
16.9034	CLAD MOTION	2	8.196	0.776	0.0	-0.566	-0.389	1.497	-0.000	0.235
16.9370	COOLANT BOILING	15	8.104	0.761	0.0	-0.592	-0.408	1.493	-0.003	0.271
16.9997	COOLANT BOILING	14	5.983	0.658	0.0	-0.623	-0.430	1.466	-0.013	0.258
17.0284	CLAD MOTION	4	5.902	0.647	0.0	-0.632	-0.438	1.500	-0.038	0.254
17.0897	CLAD MOTION	7	4.600	0.534	0.0	-0.645	-0.450	1.564	-0.203	0.268
17.1284	COOLANT BOILING	5	3.260	0.338	0.0	-0.650	-0.453	1.602	-0.435	0.273
17.1697	RELEASE GAS	11	2.179	0.010	0.0	-0.650	-0.453	1.625	-0.763	0.251
17.2297	RELEASE GAS	10	1.403	-0.519	0.0	-0.642	-0.451	1.568	-1.182	0.189
17.4309	COOLANT BOILING	3	0.889	-1.209	0.0	-0.626	-0.447	1.491	-1.677	0.050
17.4384	STOP RELEASE	4	0.871	-1.252	0.0	-0.625	-0.447	1.490	-1.714	0.044
17.4747	COOLANT BOILING	1	0.809	-1.391	0.0	-0.621	-0.446	1.493	-1.827	0.010
17.4797	CLAD MOTION	11	0.808	-1.393	0.0	-0.621	-0.446	1.493	-1.826	0.008
17.5622	CLAD MOTION	10	0.774	-1.406	0.0	-0.613	-0.445	1.519	-1.854	-0.013
17.5797	RELEASE GAS	9	0.749	-1.474	0.0	-0.611	-0.445	1.531	-1.919	-0.030
17.6897	COOLANT BOILING	8	0.663	-1.691	0.0	-0.604	-0.444	1.613	-2.127	-0.129
17.7034	STOP RELEASE	7	0.679	-1.603	0.0	-0.603	-0.444	1.633	-2.095	-0.095
17.7634	RELEASE GAS	13	0.811	-1.085	0.0	-0.593	-0.443	1.795	-1.899	0.054

Table 5 (cont'd)
Event sequence for Case 1

TIME	EVENT	CHN*	P/PO	RHO	RHOP	RHOD	RHOE	RHOV	RHOF	RHOC
17.8447	CLAD MOTION	9	1.060	-0.519	0.0	-0.589	-0.442	1.867	-1.538	0.183
17.8934	STOP RELEASE	2	1.354	-0.159	0.0	-0.591	-0.442	1.918	-1.287	0.242
18.0072	RELEASE GAS	12	7.570	0.795	0.0	-0.620	-0.446	1.864	-0.684	0.681
18.0384	PEAK REACTIVITY	0	42.984	0.960	0.0	-0.674	-0.454	1.819	-0.566	0.835
18.0434	PEAK POWER	0	46.536	0.956	0.0	-0.693	-0.456	1.810	-0.565	0.860
18.0522	FUEL MOTION	2	36.776	0.933	0.0	-0.723	-0.461	1.790	-0.572	0.898
18.0559	FUEL MOTION	4	30.773	0.923	0.0	-0.731	-0.461	1.784	-0.584	0.915
18.0597	FUEL MOTION	7	26.979	0.911	0.0	-0.737	-0.462	1.774	-0.600	0.936
18.0609	STOP RELEASE	10	25.953	0.906	0.0	-0.739	-0.463	1.773	-0.608	0.943
18.1134	CLAD MOTION	13	2.461	-0.039	0.0	-0.757	-0.464	1.771	-1.902	1.312
18.1559	RELEASE GAS	15	1.487	-0.709	0.0	-0.744	-0.463	1.915	-3.238	1.821
18.1659	FUEL MOTION	10	1.375	-0.844	0.0	-0.741	-0.463	1.953	-3.542	1.948
18.2359	CLAD MOTION	12	0.659	-2.926	0.0	-0.722	-0.463	2.093	-6.406	2.572
18.2596	FUEL MOTION	11	0.558	-3.672	0.0	-0.719	-0.463	2.065	-7.091	2.536
18.2634	RELEASE GAS	14	0.544	-3.799	0.0	-0.719	-0.463	2.058	-7.195	2.521
18.2894	TERMINATION	0	0.468	-4.626	0.0	-0.718	-0.464	1.962	-7.647	2.241

* Terminology: CHN stands for the SAS3D channel number; P/PO stands for the normalized power; RHO stands for the net reactivity; and RHOX stands for reactivity component X where X = P means programed reactivity, X = D means Doppler, X = E means axial expansion, X = V means voiding, X = F means fuel motion, and X = C means clad motion. Reactivities are in dollars.

slug re-enters the channel and rewets some very hot cladding below the molten blockage, the pressure at the lower bubble interface increases to a value near 4.5 atm and causes the gas release model to force gas and vapor back into the plenum, thus, causing the pressure in the plenum to increase. The coolant pressure in the axial node adjacent to the rupture site remains near or below 2.0 atm, and it is likely that had this pressure been used in the gas release calculation, the gas release would have been stopped before fuel motion started.

In the calculation shown in Table 5, it is assumed that gas release occurs at the middle of the top fuel node in the active core when the clad temperature is near 1300°C. The assumption that clad failure occurs at the top of the active core may be conservative, since, depending on the condition of the fuel-cladding gap, it is likely that initial clad failure might occur somewhat earlier at a point farther down in the core. The failure zone is likely to propag e upward and reach the top of the core, but by this time, the pressure in the fission gas plenum would have already been reduced somewhat. Such behaviour was observed in the R8 test for pin number 6 which had been ejected upward out of the core region. As noted in Reference 11, the top of the long axial rip was 5.0 cm below the top of the active fuel and extended downward to about 9.4 cm where the cladding effectively severed. Thus, the assumption of initial failure at the top of the core probably prolongs the time required to remove the plenum gas by some undetermined time interval. Once the release begins, the pressure in the channel rapidly increases to values as large as 5 to 6 atm. This high pressure temporarily chokes off vaporization of any sodium film that may remain on hot cladding near the bottom of the active core. In the meantime, the cladding temperature continues to increase. The high channel pressure ejects any sodium slug that

may remain in the top of the subassembly and often ejects the lower sodium slug from the bottom of the subassembly. While these events are taking place, the mass flow rate of gas from the plenum is decreasing, and the pressure in the coolant channel begins to drop nonmonotonically. As a result of the nonmonotonically dropping pressure, vaporization may resume intermittently in the lower part of the channel, and through much of the time required for the gas to be completely exhausted from the plenum, gas and vapor flow in the active core may be alternately upward and downward.

The implications of the gas release on the motion of molten cladding depend on the coupling between the clad and the streaming vapor. While the motion of gas and vapor alternates between upward and downward, when upward motion does occur, vapor velocities may be very high. As a result, with the normal flooded two-phase friction factor used in SAS3D, initial clad motion tends to be upward, sometimes leading to significant clad motion reactivity insertion rates. As noted earlier, this kind of motion is also predicted in the SAS3D analysis of the R8 TREAT test, and leads to a calculated upper cladding blockage that was not observed in the experiment. This result provided motivation for modifying the code so that the user could specify the use of nominal single phase friction coupling between clad and vapor. As already noted, when the nominal single phase friction factor is used in the R8 analysis, clad motion tends to be predominately downward and an upper cladding blockage is not predicted, a result more consistent with experimental observation. When the nominal single phase friction factor is used in the whole core analysis, the initial clad motion in most channels tends to be downward. At the time gas release stops or shortly thereafter, cladding frequently fills the coolant channel near an axial location about one third of the way up in the active core and begins to move upward, driven primarily by

the coolant vapor pressure drop. Clad does not move up coherently in all channels; the time when upward motion occurs is delayed depending on the time of gas release in the channel. This upward clad motion subsequently leads to positive reactivity insertion rates, but these rates occur at a time when the reactor is subcritical because of fuel motion in channel 6. At about the time upward clad motion is established in channel 2, fuel in channel 6, which has been initially dispersed by fission gas, begins to fall back into the core. The fuel fallback, together with the upward clad relocation, is responsible for the power increase that leads to the initiation of fuel motion in channels 2, 4, and 7.

The transient described above differs in several ways from the transient predicted in the response to question CS760.178A3. The event sequence for this latter case, Case 2, is reproduced in Table 6 for ease of reference. The first noticable effect of the larger sodium void worth in the present calculation is that initial boiling occurs about 0.8 s earlier in Case 1 than in Case 2. At the time of initial boiling, the net reactivity is 2 cents higher in Case 1 than in Case 2, but the void reactivity is nearly 4 cents higher. The lower increase in the net reactivity is caused by an increased fuel temperature resulting in a combined Doppler and axial expansion feedback with magnitude nearly 2 cents higher in Case 1 than in Case 2. The increased fuel temperature, in turn, leads to the earlier boiling time.

A second difference between the two cases is the fact that the time between initial boiling and the final shutdown in the initiating phase is more than 2.5 s longer in Case 2 than in Case 1. At least four factors may contribute to the shorter time span in the present case. The first of these is the higher sodium void worth. Based on a comparison between the present case and a case in which clad motion was not permitted, one can estimate that

Table 6
Event sequence for Case 2

TIME	EVENT	CHN*	P/PO	RHO	RHOP	RHOD	RHOE	RHOV	RHOF	RHOC
12.7655	COOLANT BOILING	6	0.821	-0.094	0.0	-0.140	-0.050	0.096	0.0	0.0
14.6697	COOLANT BOILING	2	0.819	-0.068	0.0	-0.156	-0.057	0.145	0.0	0.0
15.0561	COOLANT BOILING	4	0.817	-0.069	0.0	-0.161	-0.061	0.152	0.0	0.0
15.7772	COOLANT BOILING	7	0.851	-0.019	0.0	-0.170	-0.068	0.219	0.0	0.0
17.1048	COOLANT BOILING	10	1.226	0.234	0.0	-0.235	-0.125	0.594	0.0	0.0
17.1998	COOLANT BOILING	11	1.269	0.253	0.0	-0.242	-0.132	0.627	0.0	0.0
17.5298	COOLANT BOILING	9	1.321	0.252	0.0	-0.270	-0.159	0.681	0.0	0.0
17.7792	COOLANT BOILING	13	1.241	0.190	0.0	-0.287	-0.175	0.653	0.0	0.0
17.9242	CLAD MOTION	6	1.320	0.233	0.0	-0.297	-0.186	0.715	0.0	0.0
18.2117	COOLANT BOILING	12	2.225	0.514	0.0	-0.333	-0.223	0.999	0.0	0.071
18.6442	COOLANT BOILING	15	2.570	0.531	0.0	-0.397	-0.279	1.130	0.0	0.076
18.8732	COOLANT BOILING	14	3.002	0.561	0.0	-0.440	-0.315	1.241	0.0	0.075
19.1867	CLAD MOTION	2	2.889	0.498	0.0	-0.495	-0.366	1.282	0.0	0.076
19.3417	CLAD MOTION	4	3.770	0.594	0.0	-0.527	-0.390	1.238	0.0	0.273
19.3617	FUEL MOTION	6	3.784	0.590	0.0	-0.532	-0.393	1.233	0.0	0.283
19.4129	COOLANT BOILING	5	3.695	0.570	0.0	-0.544	-0.400	1.200	0.005	0.308
19.4930	PEAK REACTIVITY	0	4.654	0.644	0.0	-0.563	-0.411	1.207	0.003	0.408
19.5017	PEAK POWER	0	4.670	0.643	0.0	-0.566	-0.413	1.201	0.002	0.419
19.6092	CLAD MOTION	7	3.453	0.492	0.0	-0.587	-0.426	1.186	-0.110	0.428
19.6163	COOLANT BOILING	3	3.437	0.488	0.0	-0.588	-0.427	1.186	-0.123	0.441
19.7705	COOLANT BOILING	1	1.744	-0.022	0.0	-0.594	-0.434	1.145	-0.701	0.560
19.7730	COOLANT BOILING	8	1.722	-0.036	0.0	-0.594	-0.434	1.145	-0.712	0.559
20.1267	CLAD MOTION	10	0.984	-0.651	0.0	-0.579	-0.432	1.365	-1.523	0.518
20.1555	CLAD MOTION	11	1.004	-0.601	0.0	-0.578	-0.432	1.389	-1.523	0.543
20.5080	CLAD MOTION	9	1.514	0.007	0.0	-0.588	-0.433	1.565	-1.523	0.987
20.7005	CLAD MOTION	13	1.506	0.019	0.0	-0.597	-0.433	1.586	-1.523	0.986
20.9430	FUEL MOTION	2	1.989	0.259	0.0	-0.610	-0.431	1.731	-1.523	1.092
21.1105	FUEL MOTION	4	2.863	0.470	0.0	-0.629	-0.428	1.773	-1.402	1.157
21.1342	CLAD MOTION	12	2.665	0.425	0.0	-0.631	-0.428	1.760	-1.399	1.123
21.5380	FUEL MOTION	7	0.681	-1.324	0.0	-0.638	-0.425	1.848	-3.711	1.602
21.8117	CLAD MOTION	15	0.363	-3.377	0.0	-0.634	-0.426	1.864	-5.636	1.456
21.8830	TERMINATION	0	0.334	-3.742	0.0	-0.633	-0.426	1.837	-5.904	1.385

* Terminology: CHN stands for the SAS3D channel number; P/PO stands for the normalized power; RHO stands for the net reactivity; and RHOX stands for reactivity component X where X = P means programed reactivity, X = D means Doppler, X = E means axial expansion, X = V means voiding, X = F means fuel motion, and X = C means clad motion. Reactivities are in dollars.

the increased sodium void worth alone shortens the time span by somewhat more than 1 s. A second factor is the higher clad worth. It is difficult to separate this factor from the third factor which is the actual clad motion. It appears that clad motion along with the increased clad worth also shortens the time span between first boiling and reactor shutdown by somewhat more than a second. The contribution of the fourth factor, fuel fallback in channel 6, appears to be small because the fallback occurs simultaneously with a rapid increase in clad motion feedback. As a result, the power burst that occurs just after 18 s in Case 1 would have occurred even without the fuel fallback. A preliminary calculation, similar to case 1, indicates that the power excursion resulting from clad motion alone, while somewhat milder than the present excursion, is sufficient to initiate fuel motion in channels 2, 4, 7, 10, and 11 and lead to reactor shutdown on about the same time scale as in the present case.

The influence of the new neutronics data on the potential for fission-gas-driven compaction of fuel can be shown with reference to Table 7. The table shows the times between the initiation of gas release and the initiation of fuel motion for each of the driver channels. In interpreting the results, bear in mind that a clad failure temperature of 1400°C was assumed for estimating the times listed for Case 2 while a temperature of 1300°C was used in the present case (Case 1). In spite of the lower clad failure temperature in the present calculation, the times are considerably shorter than in the earlier case. While the margin is not as great as it was previously, there is ample time for gas release in the present calculation.

The fission gas parameters used in SLUMPY are the same for both Cases 1 and 2, and are based on a FRAS3[3,4,5] analysis of the best estimate case in Reference 2. They correspond to a fraction of steady-state fission gas

Table 7

Comparison of times between initiation of gas release and the initiation of fuel motion in Cases 1 and 2. Note that the clad failure temperature was 1400°C in Case 2.

SAS3D Channel Number	Case 1	Case 2
2	1.69 s	2.36 s
4	1.52 s	2.38 s
6	1.86 s	2.58 s
7	1.25 s	2.51 s
9	0.71 s*	1.96 s*
10	0.94 s	2.31 s*
11	1.09 s	2.39 s*
12	0.28 s*	1.54 s*
13	0.53 s*	1.89 s*
14	0.03 s*	0.66 s*
15	-	0.86 s*

* The time to the end of the calculation since fuel motion did not initiate in this channel.

retained in grains of 54% and a fraction of steady-state gas on the grain boundaries of 4.7%. FRAS3 calculations were redone for channel 6 using the thermal history obtained in Case 1. The gas fractions based on the new transient were found to be 70% and 2.7% respectively. Case 1 has not been rerun using the new gas fractions, but based on previous experience using the SLUMPY model, the fuel dispersal computed for channel 6 would not be expected to change significantly.

In concluding the discussion of Case 1, we note that the potential for fuel failure into liquid sodium is effectively absent. Figure 10 shows the voiding pattern in the reactor by channel at the end of the transient. It can be seen that voiding is in progress in all channels and that sodium has been completely removed from the active fuel region in all driver subassemblies except for the lower third of channels 10 and 14. Fuel motion is in progress in channel 10, but the fuel melt fraction is still below 0.1 in channel 14.

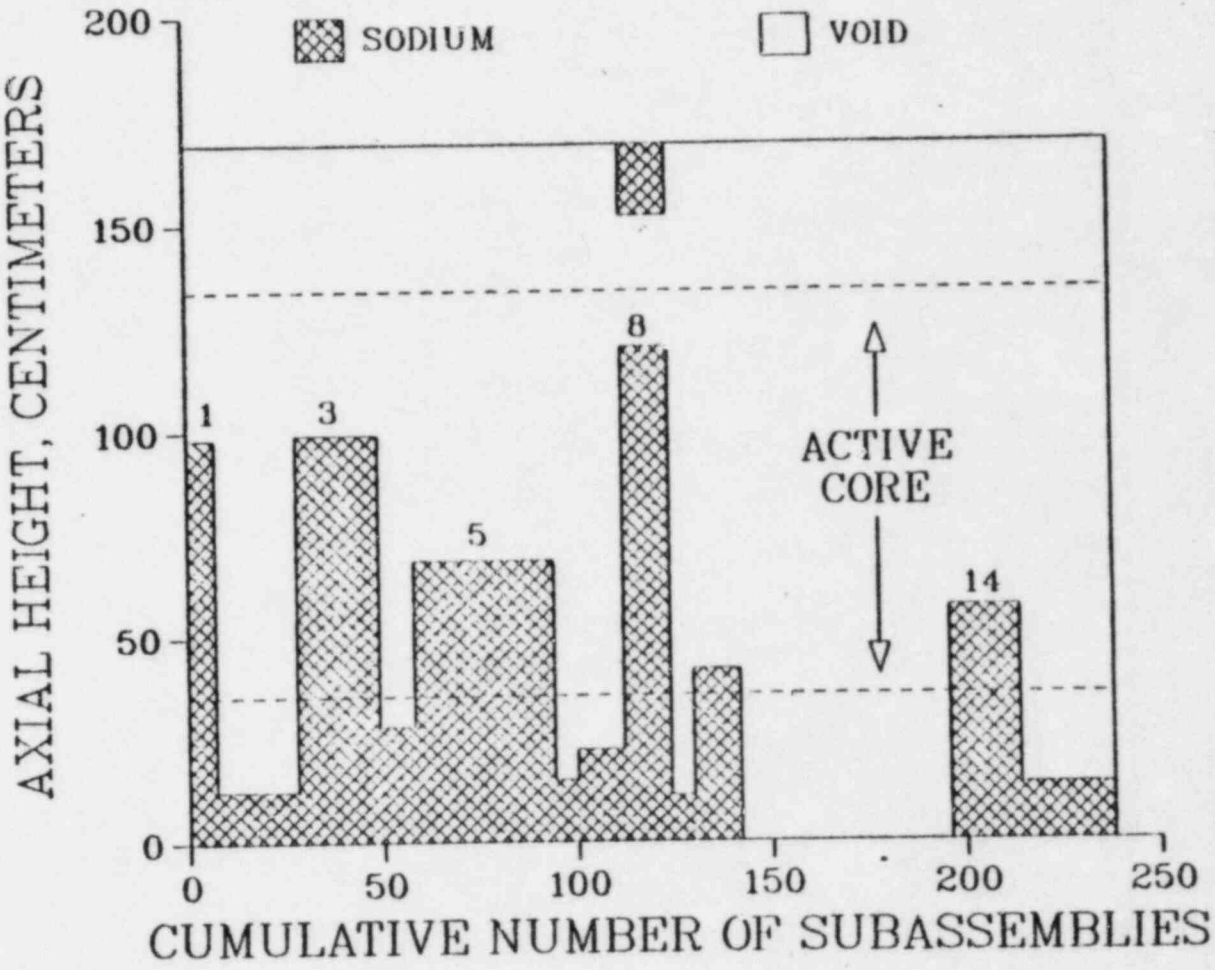

Figure 10. Sketch of the Voiding Pattern in the Reactor Core at the End of Case 1, Including the Upper and Lower Axial Blankets. (Each Histogram Bar Represents an SAS Channel, and a Few of These Are Numbered to Assist in Identification. Channels 1, 3, 5, and 8 Are Internal Blanket Subassemblies.)

Sensitivity studies have been carried out, in which the clad failure temperature was changed from 1300°C to 1400°C. The event sequence for this case, Case 3, is shown in Table 8. As expected, gas release in all channels starts later than in Case 1. This, in turn, causes events subsequent to gas release in channel 6 to be delayed compared to the times of their occurrance in Case 1. These delays are sufficient for gas release to end prior to initiation of fuel motion in five of the first six channels. The times between the start of gas release and the initiation of fuel motion is shown for these six channels in Table 9. The results show that the reduction in the time between the start of gas release and the initiation of fuel motion is not generally as large as the time delay in the start of gas release. In fact, if the reactivity had not gone slightly above prompt critical in Case 3, it is likely that all channels initiating fuel motion would have previously stopped releasing gas or have had sufficiently low pressure in the fission gas plenum so that fission-gas-driven compaction would not be a concern.

As can be seen in the event sequence for Case 3 in Table 8, channels 9, 10, 12, and 13 begin fuel motion before gas release has stopped. In the case of channel 10, the pressure in the fission gas plenum is only 3.3 atm when fuel motion starts and is not likely to play a significant role in the remainder of the transient. In the case of channels 9, 12, and 13, the pressures are respectively 11.3, 33.2, and 15.2 atm. These pressures would be high enough to influence the remainder of the transient were it not for the fact that these three channels begin fuel motion after the net reactivity has begun to decrease because of strong Doppler feedback and dispersive fuel motion in channels 2, 4, 6, and 7. To see the effects of fission-gas-driven compaction of fuel in channels 9, 10, 12, 13, and possibly 14 and 15, the compaction model introduced into SLUMPY for this purpose was utilized. The

Table 8
Event sequence for Case 3

TIME	EVENT	CHN*	P/P0	RHO	RHOP	RHOD	RHOE	RHOV	RHOF	RHOC
11.9251	COOLANT BOILING	6	0.863	-0.074	0.0	-0.151	-0.058	0.134	0.0	0.0
13.4879	COOLANT BOILING	2	0.902	-0.013	0.0	-0.172	-0.068	0.227	0.0	0.0
13.8538	COOLANT BOILING	4	0.866	-0.059	0.0	-0.180	-0.073	0.193	0.0	0.0
14.3099	COOLANT BOILING	7	0.880	-0.038	0.0	-0.187	-0.079	0.228	0.0	0.0
15.6665	CLAD MOTION	5	1.525	0.330	0.0	-0.273	-0.152	0.755	0.0	0.0
15.6815	RELEASE GAS	5	1.540	0.335	0.0	-0.275	-0.153	0.758	0.0	0.006
15.7465	COOLANT BOILING	10	1.563	0.337	0.0	-0.283	-0.161	0.776	0.0	0.005
15.8260	COOLANT BOILING	11	1.502	0.301	0.0	-0.291	-0.168	0.768	0.0	-0.007
16.0935	COOLANT BOILING	9	1.568	0.301	0.0	-0.321	-0.196	0.866	0.0	-0.047
16.3810	STOP RELEASE	6	1.620	0.303	0.0	-0.349	-0.223	0.947	0.0	-0.072
16.4279	COOLANT BOILING	13	1.813	0.375	0.0	-0.354	-0.227	1.034	0.0	-0.078
16.6627	COOLANT BOILING	12	2.489	0.504	0.0	-0.399	-0.263	1.271	0.0	-0.105
16.8060	RELEASE GAS	2	2.919	0.561	0.0	-0.427	-0.283	1.201	0.0	0.070
16.9560	CLAD MOTION	2	7.767	0.798	0.0	-0.511	-0.344	1.391	0.0	0.263
16.9835	RELEASE GAS	4	9.003	0.815	0.0	-0.536	-0.362	1.415	0.0	0.298
17.0360	CLAD MOTION	4	7.859	0.767	0.0	-0.576	-0.393	1.436	0.0	0.299
17.0435	FUEL MOTION	6	8.091	0.771	0.0	-0.581	-0.397	1.442	0.0	0.308
17.0660	COOLANT BOILING	15	7.765	0.754	0.0	-0.596	-0.409	1.459	-0.000	0.299
17.1072	RELEASE GAS	7	7.310	0.726	0.0	-0.616	-0.426	1.489	-0.001	0.280
17.1610	COOLANT BOILING	14	7.386	0.715	0.0	-0.640	-0.445	1.553	0.009	0.238
17.1935	CLAD MOTION	7	5.512	0.606	0.0	-0.651	-0.454	1.588	-0.097	0.220
17.3147	COOLANT BOILING	5	1.920	-0.130	0.0	-0.656	-0.459	1.602	-0.821	0.203
17.4360	COOLANT BOILING	3	1.321	-0.569	0.0	-0.646	-0.456	1.538	-1.083	0.078
17.4460	RELEASE GAS	11	1.263	-0.637	0.0	-0.645	-0.456	1.533	-1.136	0.066
17.4510	COOLANT BOILING	1	1.218	-0.696	0.0	-0.644	-0.456	1.529	-1.181	0.056
17.5860	RELEASE GAS	10	0.905	-1.172	0.0	-0.630	-0.454	1.543	-1.552	-0.077
17.6147	CLAD MOTION	11	0.885	-1.193	0.0	-0.628	-0.454	1.565	-1.564	-0.112
17.6422	CLAD MOTION	10	0.880	-1.174	0.0	-0.625	-0.454	1.575	-1.541	-0.129
17.7972	STOP RELEASE	4	1.500	-0.155	0.0	-0.624	-0.453	1.611	-1.215	0.526
17.9410	CLAD MOTION	9	4.692	0.629	0.0	-0.640	-0.456	1.733	-0.738	0.730
17.9622	COOLANT BOILING	8	5.059	0.649	0.0	-0.646	-0.457	1.777	-0.725	0.700
18.0147	RELEASE GAS	9	3.329	0.444	0.0	-0.654	-0.459	1.922	-0.953	0.588

Table 8 (cont'd)
Event sequence for Case 3

TIME	EVENT	CHN*	P/PO	RHO	RHOP	RHOD	RHOE	RHOV	RHOF	RHOC
18.0272	STOP RELEASE	2	2.801	0.335	0.0	-0.654	-0.459	1.959	-1.077	0.566
18.1085	RELEASE GAS	13	1.666	-0.126	0.0	-0.648	-0.459	2.171	-1.816	0.627
18.1347	CLAD MOTION	13	1.569	-0.190	0.0	-0.648	-0.459	2.198	-1.984	0.703
18.2222	STOP RELEASE	7	6.503	0.723	0.0	-0.665	-0.461	2.156	-1.492	1.184
18.2360	FUEL MOTION	2	13.645	0.873	0.0	-0.677	-0.462	2.141	-1.424	1.294
18.2397	STOP RELEASE	11	19.285	0.914	0.0	-0.682	-0.462	2.139	-1.406	1.325
18.2470	FUEL MOTION	4	46.656	0.977	0.0	-0.700	-0.465	2.126	-1.372	1.388
18.2501	FUEL MOTION	7	88.822	1.003	0.0	-0.716	-0.465	2.124	-1.357	1.418
18.2523	PEAK REACTIVITY	0	154.934	1.013	0.0	-0.733	-0.465	2.124	-1.350	1.437
18.2549	FUEL MOTION	10	258.308	1.003	0.0	-0.770	-0.464	2.125	-1.343	1.456
18.2555	FUEL MOTION	11	274.136	0.997	0.0	-0.781	-0.464	2.125	-1.342	1.460
18.2561	PEAK POWER	0	280.618	0.992	0.0	-0.791	-0.464	2.125	-1.342	1.464
18.2567	FUEL MOTION	9	278.637	0.985	0.0	-0.803	-0.463	2.126	-1.343	1.468
18.2586	FUEL MOTION	13	216.685	0.962	0.0	-0.834	-0.461	2.127	-1.351	1.480
18.2593	FUEL MOTION	12	183.196	0.952	0.0	-0.843	-0.460	2.128	-1.357	1.485
18.2717	RELEASE GAS	12	3.673	0.040	0.0	-0.866	-0.455	2.145	-2.385	1.601
18.3480	CLAD MOTION	12	0.416	-8.591	0.0	-0.808	-0.456	2.339	-11.583	1.917
18.3730	STOP RELEASE	10	0.366	-10.027	0.0	-0.798	-0.456	2.375	-13.283	2.135
18.4168	RELEASE GAS	15	0.346	-10.359	0.0	-0.791	-0.457	2.404	-13.696	2.180
18.4893	TERMINATION	0	0.311	-11.238	0.0	-0.799	-0.457	2.103	-14.183	2.097

* Terminology: CHN stands for the SAS3D channel number; P/PO stands for the normalized power; RHO stands for the net reactivity; and RHOX stands for reactivity component X where X = P means programed reactivity, X = D means Doppler, X = E means axial expansion, X = V means voiding, X = F means fuel motion, and X = C means clad motion. Reactivities are in dollars.

Table 9
Comparison of times between initiation of gas release and the initiation of fuel motion in Cases 1 and 3.

SAS3D Channel Number	Case 1	Case 3
2	1.69 s	1.43 s
4	1.52 s	1.26 s
6	1.86 s	1.36 s
7	1.25 s	1.14 s
10	0.94 s	0.67 s
11	1.09 s	0.81 s

event sequence for the resulting case, Case 4, is almost identical to that for Case 3. The dispersive fuel motion from channels 2, 4, 6, 7, 10, and 11 (representing 84 subassemblies) was sufficient to overcome the reactivity insertion rates produced by the compacting fuel in channels 9, 12, and 13 (representing 36 subassemblies). Channels 14 and 15 did not initiate fuel motion and had peak fuel melt fractions between 0.35 and 0.4 when the transient ended. Table 10 shows the work-energy obtained when super-saturated fuel is expanded adiabatically to a final pressure of 1 atm for Cases 1, 3, and 4. These results show that the LOF transient using the modeling assumptions of Case 1 is not sensitive to the choice of the clad failure temperature used in the fission gas release calculations.

Table 10
Work-energies based on adiabatic expansions of super-saturated fuel to a final pressure of 1 atm.

Case	Work-Energy, MJ
1	0.6
3	4.3
4	5.6

IV. Conclusions

The assessment of sodium void coefficient uncertainties has resulted in an increase in the nominal values of sodium void and clad material worths in the CRBRP heterogeneous core. These changes have increased the sensitivity of whole core analysis results to the modeling of important phenomenology. The importance of representing fuel disruption and dispersal consistently with the experimental database has been previously established. It has been demonstrated in this report that similar experimentally-based models can be developed in the areas of molten cladding relocation, the effect of release of plenum fission gas on sodium vapor dynamics and clad motion, and failure of irradiated cladding under the fission gas plenum pressures.

The whole core best estimate analyses have shown that with such experimentally validated models, a mild power burst with near zero energetics is expected. This conclusion is valid even in the unlikely event that the plenum fission gas can act to compress the disrupting fuel. Parametric variations on clad failure and plenum gas release, and molten cladding relocation show very mild sensitivities in initiating phase energetics. The potential for significant energetics appears to require pessimistic phenomenological modeling that is not supported by the present experimental database, and is therefore beyond that appropriate for a realistic assessment of the accident energetics. The likelihood of energetics approaching the SMBDB value is very remote.

Appendix A

Modifications to the SAS3D Boiling Module to Account for Release of Plenum Gas into a Boiling Region

The gas voiding model in Version 1.0 of SAS3D is mainly applicable to voiding due to pin failure and gas release before the onset of boiling. If a pin fails in a boiling region, this model will calculate the flow of gas from the gas plenum to the failure point, but the only effect on the voiding is a reduction in the condensation coefficient of the vapor. This model has been modified to provide a better treatment of the impact of gas release into a boiling region.

In the modified model, gas released into a vapor bubble is treated as an additional equivalent vapor source in the boiling model. This additional vapor source is added at the one axial node where the pin rupture occurs. Since the molecular weight of fission product gas is different from that of sodium vapor, the mass of the gas leaving the rupture must be converted into an equivalent vapor mass for use in the boiling calculation. In the SAS3D boiling model, a vapor bubble is treated as either a small bubble, with uniform vapor pressure, or a larger bubble containing pressure gradients due to streaming vapor. For gas released into a small bubble, the product, pV, of pressure times volume is conserved when the gas is converted to vapor. For a perfect gas

$$pV = mRT \qquad (1)$$

so

$$m_g R_g T_g = m_v R_v T_v \qquad (2)$$

where

m_g = mass of gas leaving the rupture,

m_v = equivalent mass of the vapor source,

R_g = gas constant for the gas,

R_v = equivalent gas constant for sodium vapor

T_g = temperature of the gas leaving the rupture, assumed to be equal to the fuel surface temperature at the rupture point, and

T_v = vapor temperature at the rupture point.

Note that T_g and T_v must be absolute temperatures (K). Equation 2 gives

$$m_v = \frac{m_g R_g T_g}{R_v T_v} \qquad (3)$$

The vapor gas constant, R_v, is calculated as

$$R_v = \frac{p_v}{\rho_v T_v} \tag{4}$$

where ρ_v is the saturation vapor density and p_v is the saturation pressure at temperature T_v.

For gas released into a large vapor bubble, the friction pressure drop due to streaming gas or vapor is conserved. The friction pressure drop is

$$\Delta p_f = f \frac{G^2}{2\rho} \frac{L}{D} \tag{5}$$

where

f = friction factor,
G = mass flux
ρ = density,
L = length, and
D = hydraulic diameter.

Therefore,

$$\frac{G_v^2}{2\rho_v} f_v \frac{L}{D} = \frac{G_g^2}{2\rho_g} f_g \frac{L}{D} \qquad (6)$$

Differences between the vapor and gas friction factors are neglected. Also, G is assumed to be proportional to the mass released at the rupture, so

$$\frac{m_v^2}{2\rho_v} = \frac{m_g^2}{2\rho_g}. \qquad (7)$$

or

$$m_v = m_g \sqrt{\frac{\rho_v}{\rho_g}} = m_g \sqrt{\frac{R_g T_g}{R_v T_v}} \qquad (8)$$

For a small bubble, the heat flow to the bubble during a time step has a term ΔE_{to} added to the term E_{to} of Eq. 131 in ANL-8138[37]. This term is given by

$$\Delta E_{to} = (m_{gp1} - m_{gp2}) \frac{R_g T_g \lambda_v}{R_v T_v} \qquad (9)$$

where

m_{gp1} = mass of gas in the plenum at the beginning of the step

m_{gp2} = plenum gas mass at the end of the step and

λ_v = sodium heat of vaporization.

The FORTRAN variable name for E_{to} is DQT(1), and the term is added in subroutine TSC43A.

For gas release into a larger bubble, a term ΔQ_e is added to the heat flux from the clad to the coolant (see Eq. 153 of ANL-8138) at the rupture node in subroutine TSC4A. This term is

$$\Delta Q_e = (m_{gp1} - m_{gp2}) \frac{R_g T_g}{R_v T_v} \frac{\lambda}{\Delta t A_{cc} \Delta z} \qquad (10)$$

where

Δt = time step size,

A_{cc} = coolant flow area, and

Δz = node size

The boiling module in version 1.0 of SAS3D will stop the code if a vapor bubble extends out the bottom of the subassembly. This is because some FORTRAN subscripts for arrays used in the vapor pressure gradient calculation

would be equal to 0 if the bubble interface is below the lowest channel node (node 1), and a subscript of 0 is not allowed in FORTRAN. Gas release into a boiling region can often lead to voiding out the bottom of the channel, so the code was modified slightly to handle this case. Now if a bubble extends below the bottom of the channel, the lowest clad and structure node are ignored in the coolant calculation, and the inlet coolant temperature is used for the clad and structure temperatures at the liquid-vapor interface. The lowest vapor node then extends from the liquid-vapor interface up to node 2. By ignoring node 1 in this case, the subscripting problem is bypassed, and the calculation can continue.

Appendix B

Two-Fluid Model Analyses of Plenum Fission Gas Release

The SAS3D code is limited in its ability to treat the release of plenum fission gas into a sodium vapor filled channel. The theoretical basis for the current treatment has been provided in Appendix A. To confirm the modeling and results from SAS3D and to insure the model is conservative, an independent analysis of the plenum gas ejection scenario was undertaken. No single analysis capability was available that treated all aspects of this problem and, consequently, two methodologies from the PLUTO2 code and the TRANSIT-HYDRO code were employed which treated several factors not included in SAS3D. The qualitative agreement between these three methodologies provides confidence in the SAS3D treatment and the quantitative comparisons indicate tha the SAS3D treatment is, indeed, conservati').

B.1. TRANSIT-HYDRO Results

To evaluate the impact of approximations made in modeling the plenum fission gas injection process with the SAS3D coolant dynamics module, the TWOFLU module of the TRANSIT-HYDRO computer code has been used to simulate plenum fission gas injection into a partially voided subassembly. The TWOFLU formulation is based on a two field (liquid and vapor), three component (fuel, clad, coolant) structure in which each field has an independent velocity, and each component within a field has an independent internal energy. In addition, mass conservation is maintained for each component in each field. For the fission gas injection simulation, this permits independent tracking of the fission gas and coolant vapor components, and eliminates the need for energy and mass mixing. The particular issue addressed here is the timing and

extent of downward fission gas penetration, and the validity of the assumption of the loss of condensation potential following cladding rupture in the SAS3D coolant dynamics model.

Initial conditions for the TWOFLU simulation were taken as those predicted by SAS3D in channel 2 at the time of cladding rupture for the best estimate EOC-4 loss-of-flow analysis described in Section III. These conditions included geometry (channel length, flow area, liquid slug location, coolant film thickness and location), as well as thermal (axial temperature distributions in cladding, liquid slug, and coolant vapor), and hydrodynamic conditions (liquid slug and coolant vapor velocities). Thermodynamic and transport properties for all materials were taken from those employed in SAS3D. Momentum frictional modeling for the liquid and vapor were also taken from SAS3D, including the two-phase multiplier employed to represent the effect of liquid coolant films. To describe the gas injection process, the plenum gas pressure and temperature formulation, as well as the gas flow formulation (subroutine PIPFLO) used in SAS3D were implemented intact in TWOFLU. The time history for the pressure boundary condition at the subassembly inlet and outlet were taken from the best-estimate SAS3D LOF analysis described in Section III.

Given these initial and boundary conditions, TWOFLU predicts channel pressurization and liquid slug reversal similar to SAS3D. Figure B1 compares the channel pressure history following clad rupture at the rupture site as predicted by SAS3D,TWOFLU and PLUTO2. The comparison shows that TWOFLU predicts a somewhat higher and more sustained pressure pulse than that predicted by SAS3D. Close examination of analysis results shows that this is due to much lower gas temperatures predicted by SAS3D. Inclusion of gas/structure heat transfer effects would tend to lower the TWOFLU-predicted temperatures,

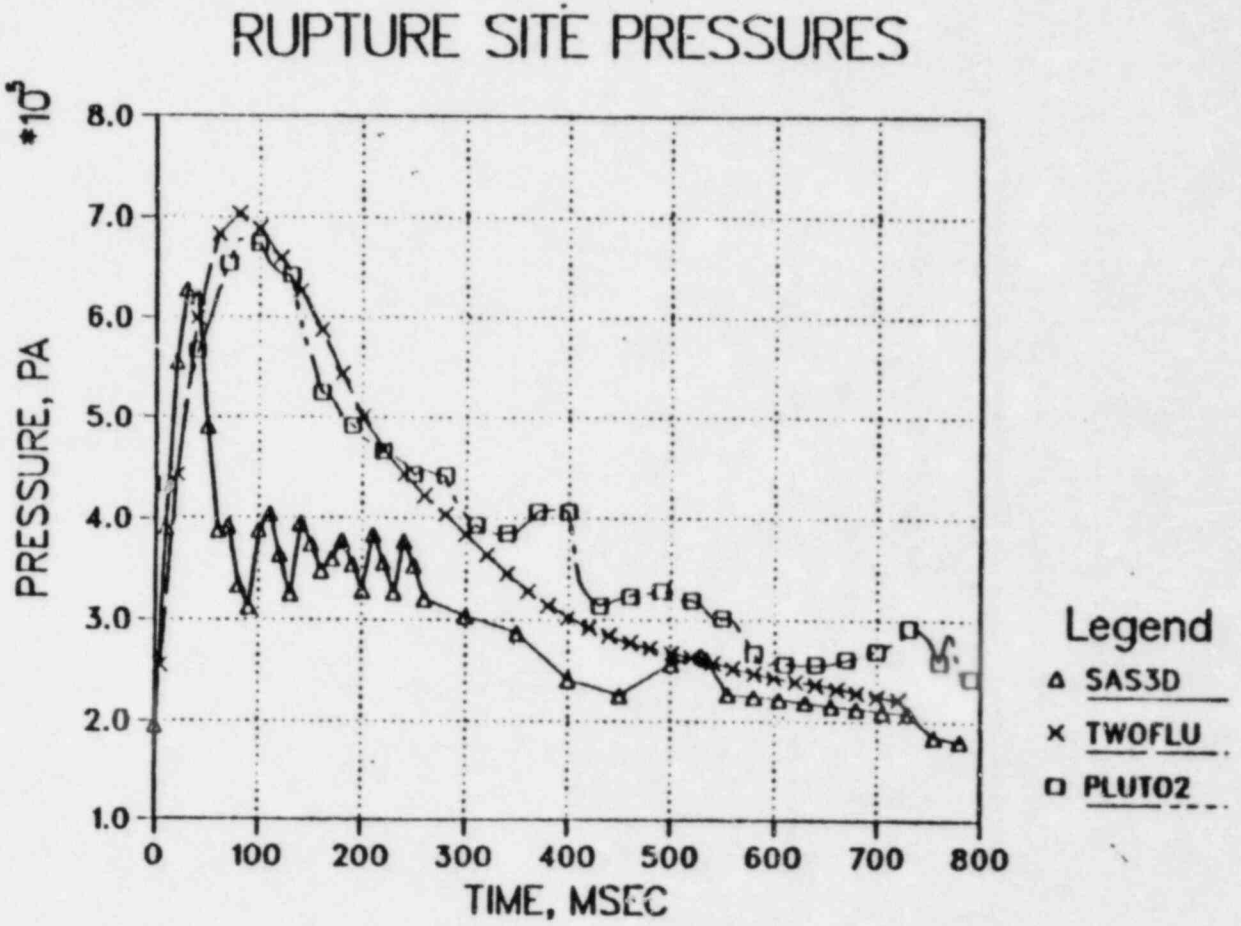

Figure B1. Rupture Site Pressure History Comparison

but not to the levels predicted by SAS3D.

The TWOFLU pressure distribution history shown in Fig. B2 causes a more rapid expulsion of the lower liquid slug than is predicted by SAS3D. In addition, the slug motion is more extensive (it is expelled from the bottom of the subassembly), and slug re-entry is delayed compared to SAS3D. This effectively lengthens the time frame for negative vapor velocities. Sensitivity studies have shown that augmentation of the subassembly inlet pressure by approximately 0.1 MPa (1 atmosphere) in the TWOFLU calculation results in slug re-entry times close to the SAS3D-predicted value.

The TWOFLU analysis shows that downward penetration of the plenum fission gas is rapid and extensive. Figure B3 shows the TWOFLU-predicted mass fraction distribution for fission gas following clad rupture. During this time, the liquid slug has reversed and is being expelled due to the fission gas pressurization. As the figure shows, even at early times fission gas has effectively penetrated down to the liquid slug interface, compressing a small amount of coolant vapor trapped below the rupture site. In addition, the fission gas has swept all of the coolant vapor formerly above the rupture site out through the top of the subassembly.

Based on the TWOFLU analysis summarized here, it can be concluded that in the event of clad rupture and plenum fission gas blowdown in channel 2 of the best-estimate LOF analysis of Section III, the released fission gas rapidly pressurizes and fills the channel. This analysis indicates that the assumptions made concerning coolant vapor condensation reduction due to fission gas blanketing of liquid coolant films in the SAS3D coolant dynamics model are reasonable and justified. In addition, this analysis indicates that channel pressurization may be somewhat higher than would be predicted by SAS3D. This would tend to enhance the potential for downward molten cladding

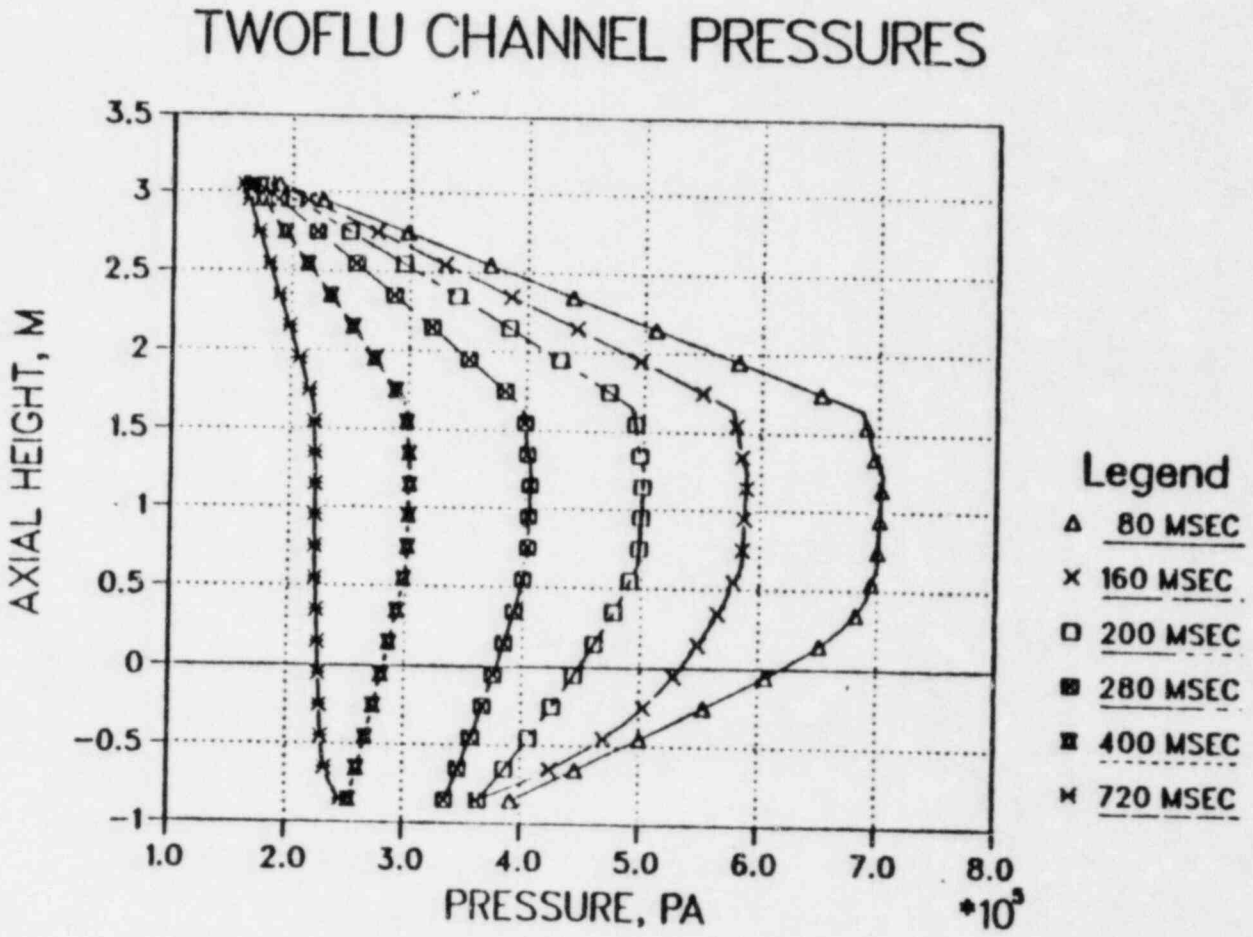

Figure B2. TWOFLU Predicted Channel Pressure Distribution History

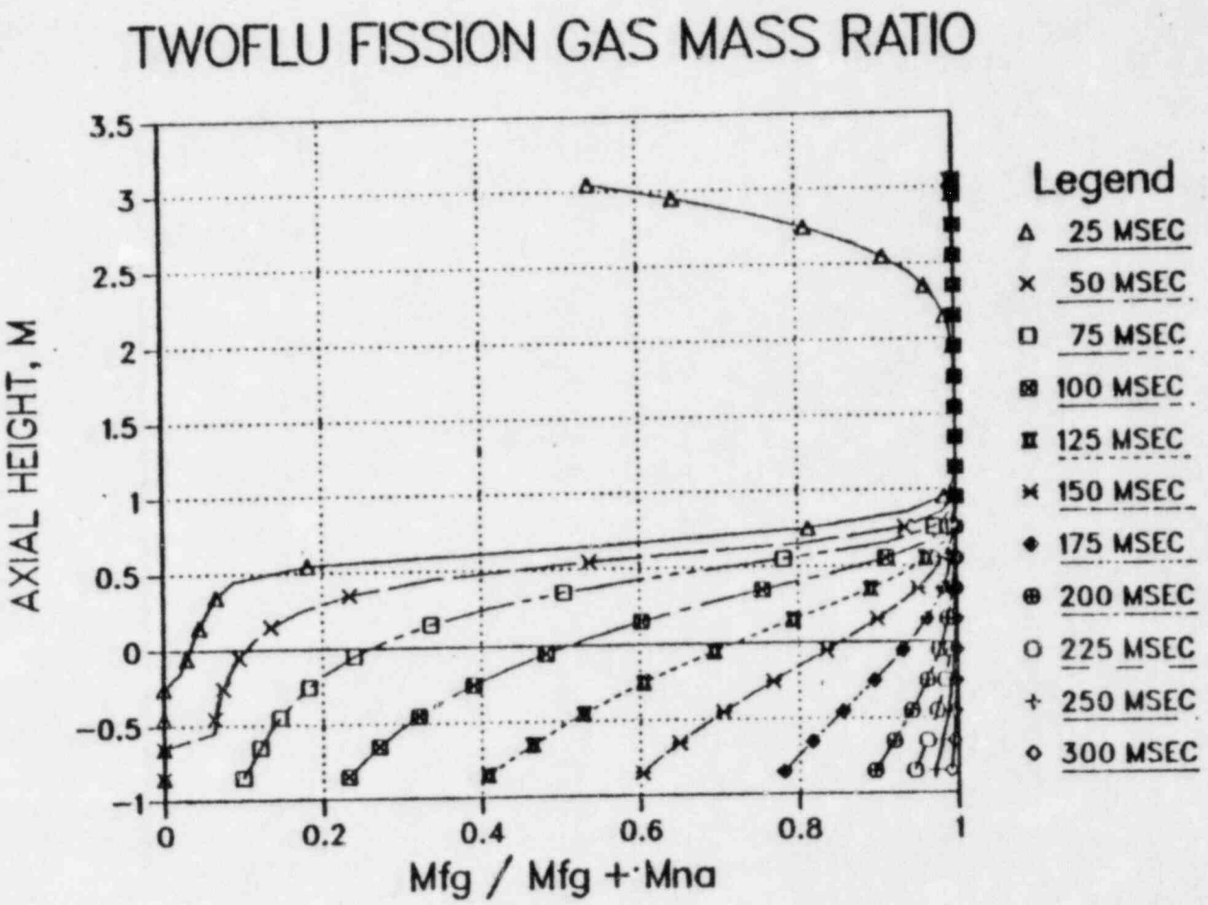

Figure B3. TWOFLU Predicted Fission Gas Distribution History

motion by lengthening the time frame for negative gas velocities. This observation is consistent with the experimental results seen in the R8 test (no upper blockage, downward clad motion) and supports the assumption of nominal single phase frictional coupling in SAS3D/CLAZAS.

B.2. PLUTO2 Results

An investigation into the effect of plenum fission-gas release on the channel flow behavior was also made with a special version of the SAS4A/PLUTO2 code. This was done in order to verify the new SAS3D modeling of plenum gas release into a boiling channel. The SAS3D base case calculation, which uses the new fission-gas/boiling model, calculates a downward motion of the vapor-gas mixture in the active core region for about a hundred milliseconds following the onset of plenum gas release. In the model the plenum gas injected into the channel is replaced by an appropriate amount of Na vapor and the sodium vapor condensation for the entire channel is set to a small value. The validity of these assumptions was investigated in this study with SAS4A/PLUTO2 which which has the capability of treating sodium and fission gas separately.

Although the better known features of the PLUTO2 module are the calculation of in-pin and channel fuel motion, it also has a fairly detailed treatment of two-phase sodium and fission-gas flow in the coolant channel. A stagnant liquid sodium film which can evaporate or be entrained by vapor flow is also modeled. In the current application the in-pin fuel motion and fuel ejection from the fuel pins was turned off. Plenum gas was injected into the coolant channel at a rate similar to that calculated by the SAS3D base case for channel 2. All geometrical and thermo-hydraulic data used in the single channel SAS4A/PLUTO2 calculation were the same as the data for channel 2 in the SAS3D whole core base case. The power and inlet pressure history

necessary for the single channel calculations were also from the SAS3D whole-core calculation.

Extensive sodium boiling and voiding took place in the current calculations before cladding failure was assumed to occur at the top of the active core when the clad midwall temperature at this location had reached 1300°C. The PLUTO2 calculation with the plenum fission gas injection was then initiated.

The PLUTO2 calculated pressure history at the rupture site is shown in Fig. B1 together with the SAS3D and the TWOFLU calculations. Both PLUTO2 and TWOFLU predict a longer lasting and higher pressure peak during the first 300 msec because both models can account for heat transfer from hot, dried-out clad to the gas in the coolant channel, whereas the SAS3D fission gas/boiling model does not account for any heat transfer from the clad at any node where the film has dried out. This causes the gas or superheated vapor temperature in PLUTO2 and TWOFLU to be several hundred degrees Kelvin hotter than in SAS3D and also makes the pressures in PLUTO2 and TWOFLU higher. At the later times both PLUTO2 and SAS3D show pressure increases which are caused by the sodium film vaporization at the lower end of the active core. In Fig. B4 the lower sodium slug interfaces calculated by SAS3D and PLUTO2 are compared. The PLUTO2 predicted slug ejection is more rapid and lasts longer than in SAS3D because of the higher pressure calculated by PLUTO2. The PLUTO2 calculated pressure distributions in the coolant channel at different times are shown in Fig. B5. The bottom of the active core is at about 0.34 m and the top of the active core, where the plenum gas injection takes place, is at about 1.25 m. The pressure distribution at 80 msec shows a peak at the plenum gas ejection site which corresponds to the maximum pressure achieved in this run. This overpressure caused the vapor/gas flow below the failure site to move

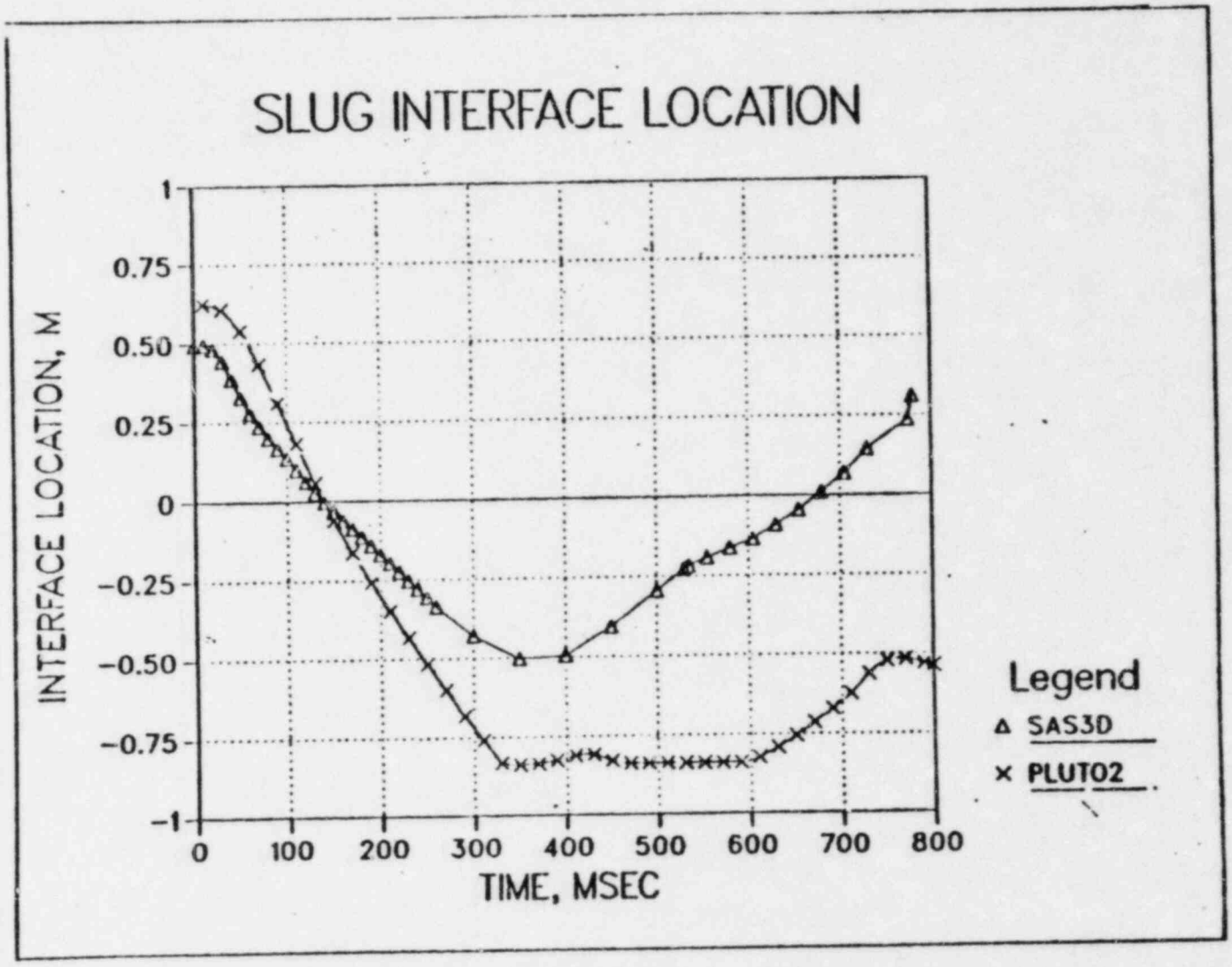

Figure B4. Lower Sodium Slug Interface Comparison

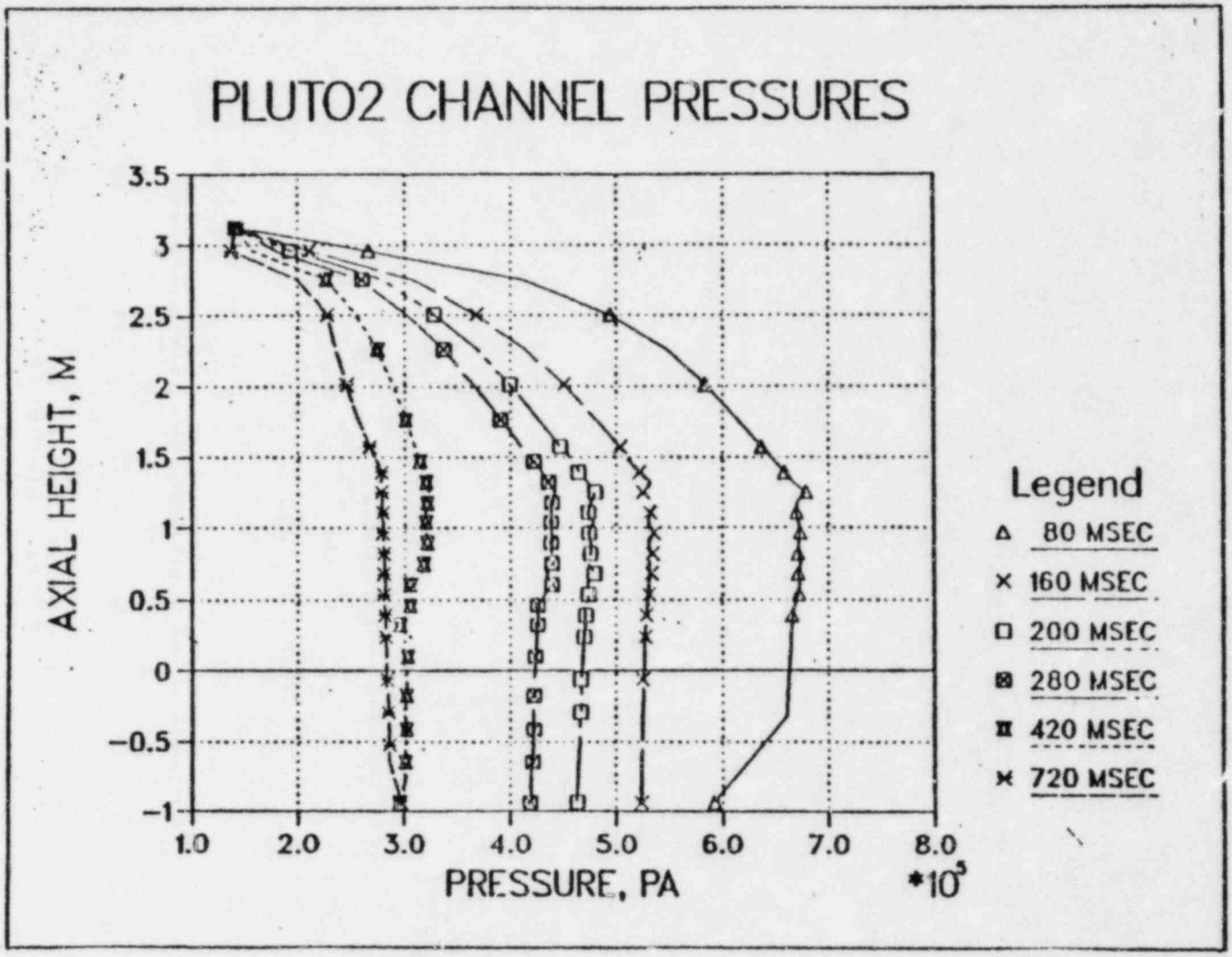

Figure B5. PLUTO2 Predicted Channel Pressure Distribution History

downwards and also led to rapid flow reversal of the lower liquid slug which can be seen in Fig. B4. The pressure distribution at 160 msec was decreased due to the upward streaming of the gas and the rapid downward motion of the lower sodium slug which is uncovering cold clad and structure in the inlet region. By 420 msec the pressure gradient below an axial location of 1 m is still downward preventing the gas vapor flow velocity below this region from becoming positive. By 720 msec the fission gas injection pressure has dropped below the inlet pressure causing a slight pressure tilt towards the outlet in the active core region. Liquid sodium film evaporation and sodium vapor condensation do not play a dominant role during the first 720 msec. The sodium film vaporization occurring at around 0.6 m keeps the pressure level at that location somewhat higher than predicted by TWOFLU at 280 and 420 msec.

In Fig. B6 the ratio of fission-gas mass over fission-gas mass + sodium vapor mass is shown at different locations and times. The two symbols shown for each curve depict the axial extent of the fission-gas region which corresponds to the boiling region at times greater than 30 msec. At later times the fission gas completely dominates the sodium vapor in the dried-out region between 0.6 and 1.25 m and also in the lower blanket and inlet region where relative cold, low density sodium vapor exists. Between 0.25 and 0.6 m as well as above 1.25 m liquid sodium film vaporization leads to the higher density sodium vapor which is noticeable on this mass ratio plot. Because the fission gas is spreading quite rapidly in this PLUTO2 calculation, it can be concluded that the SAS3D assumption of using a very small condensation coefficient is reasonable because most of the pressure in this calculation is actually due to the pressure of the noncondensible fission gas.

The SAS3D prediction of a sodium vapor flow reversal lasting only a hundred milliseconds is significantly shorter than the PLUTO2 prediction of

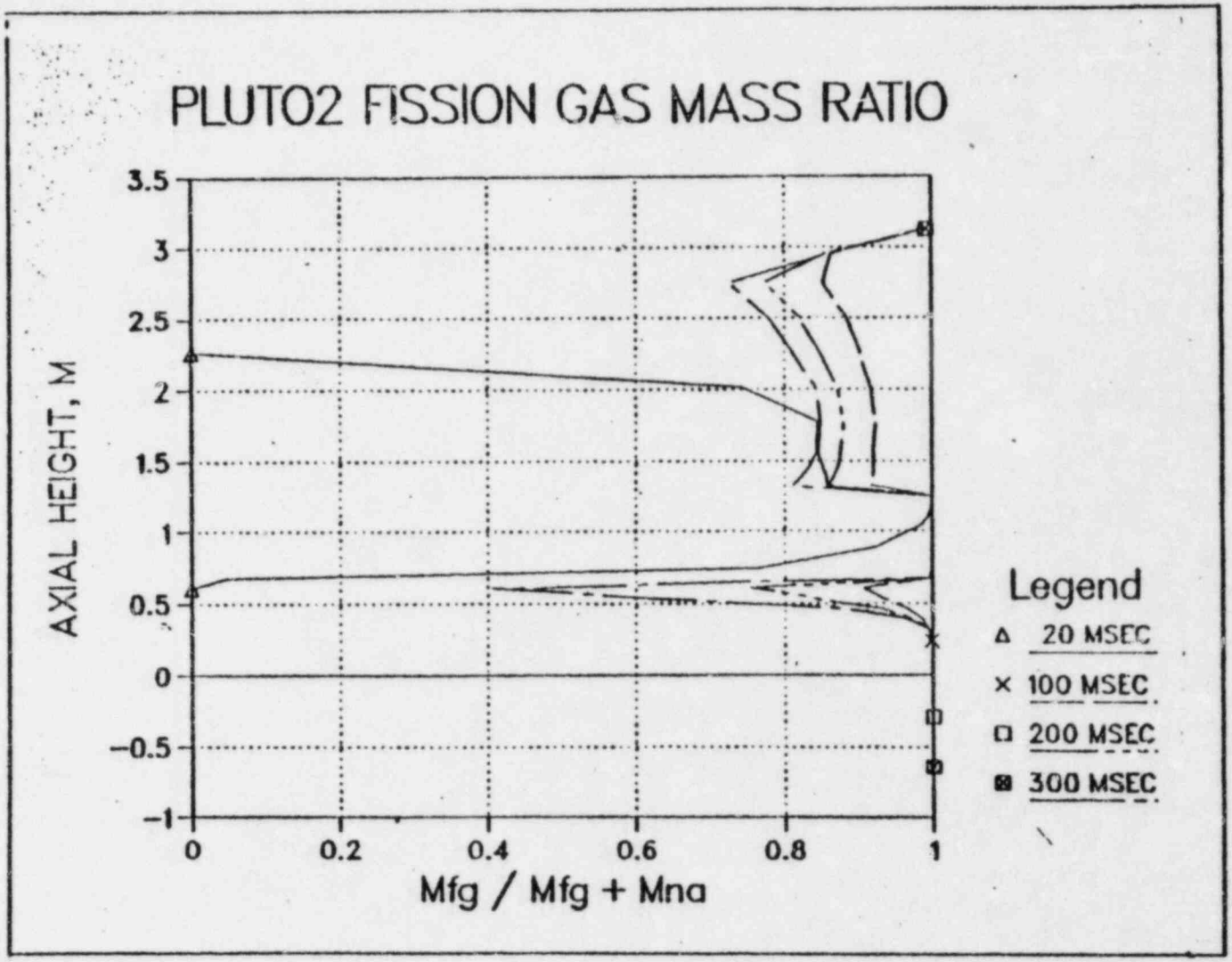

Figure B6. PLUTO2 Predicted Fission Gas and Sodium Vapor Mass History

about 400 msec. However, the SAS3D prediction is conservative because it leads to a more limited downward clad motion than a calculation with a more extensive vapor flow reversal. The main reason for the shorter lasting flow reversal is probably the lack of heat flow from dried-out clad in the SAS3D model. Moreover, it may be that the small condensation coefficient applied to the converted gas in SAS3D is still causing significant condensation and loss of gas mass over longer times.

An attempt was also made to investigate the effect of intra-subassembly incoherencies in the clad failure. This was done by injecting the plenum gas into the channel at about one quarter of the initial injection rate of the previous case. This injection lasted for 1200 msec compared to 550 msec in the previous case but led to the same total gas injection. The same inlet pressure history was used as in the previous case. The time period of negative or low vapor flows in the active core region lasted for more than 1 sec which is more than twice the value of the previous case. Apparently keeping the pressure in the gas injection node above the inlet pressure for a longer time has more impact than having a higher initial pressure which drops below the inlet pressure more rapidly. This indicates that the assumption of releasing the plenum gas from all pins simultaneously is also conservative with regard to the potential upward molten of the cladding.

Appendix C

SAS3D Modifications Required to Analyze TREAT R-Series Coolant Hydraulics

On the R8 test, a flow orifice was put in the coolant inlet pipe upstream from the test section to simulate the pressure drop of the inlet orifice in FFTF subassemblies. This orifice is normally modelled with an inlet orifice coefficient in SAS3D. In SAS3D calculations for R8, the gas release following pin rupture leads to voiding of the whole test section and expulsion of the lower liquid slug from the bottom of the subassembly. When the lower liquid slug is below the subassembly inlet, SAS3D does not account for orifice or friction pressure drops in computing the motion of the liquid. The motion is based only on inertia, as driven by the difference between the inlet plenum pressure and the bubble pressure above the liquid slug. In the R8 test, the inlet orifice was located far enough upstream that the gas will never void through the orifice, so the orifice pressure drop should always be accounted for, even if SAS3D predicts expulsion of the lower liquid slug from the bottom of the subassembly.

For use in the R8 analysis, a special version of subroutine TSC2 was produced. In this routine, the inlet orifice pressure drop is accounted for in the equation for the motion of the lower liquid slug, even after the liquid slug has blown out the bottom of the subassembly. The load module for this modified routine is stored in data set C112.B22404.SAS3DMIS. LØAD(TSC2R8) on the ANL computer system. The modifications, in UPDAT format, used to produce this routine from the SAS3D version 1.0 source are listed in table C1.

Table C1
TSC2 Modification for R8 Calculations

```
 1 0 0 1 0 0
*IBM
*NOLIST
*ORIGIN 2
*REWIND 2
*SUBS TSC2.192 TSC2.194
C           SLUG BLOWN OUT BOTTOM, INCLUDE ORIFICE FOR R8
       XIOR1(K)=XKO1
       XIOR2(K)=XKO2
       SGN=1.0D0
       IF (G1(K).LT.0.0D0) SGN-SGN
       AA0(K)=SGN*0.5D0*(XIOR1(K)+XIOR2(K))*G1(K)**2+PDCM*(PTP1(K)-PBT1(K
       1 ) )
       BB0(K)=SGN*XIOR2(K)*G1(K)
       DG0(K)=-DELT*AA0(K)/(XLL(K)+BB0(K)*DELT)
*FINI
*END
```

Appendix D

Calculation of Plenum Gas Blowdown Coupled with Pressure-Driven Fuel Motion

A simple finite-difference code was written to calculate plenum blowdown, coupled with downward motion of the fuel and (optional) upward motion of the plenum. The escape of gas from the plenum region is calculated from the relation given by Chawla et. al. for isothermal flow[38]. It can be shown from eqs. 25 and A.6 of that reference that the rate of pressure change is given by

$$\dot{P} = -P \left(\frac{RT}{2}\right)^{1/2} \frac{A_g}{V} \left[\frac{1 - \beta^2}{F - \ln\beta}\right]^{1/2} , \qquad (1)$$

where P is the plenum pressure, R is the gas constant, T is the Kelvin temperature, A_g is the flow area of the gap, V is the plenum volume, β is the ratio of the channel pressure to the plenum pressure, and F is given by

$$F = 2\ell f_g / D_g \qquad (2)$$

Here ℓ is the length of the flow path, f_g is the friction factor (taken to be constant, at 0.01, after Chawla), and D_g is the hydraulic diameter (D_g = .0284).

The geometry is depicted in Fig. D1, which shows the plenum region overlapping the blanket fuel a distance ℓ, (initially, ℓ = 14 inches, or 35.56 cm). The initial volume of the plenum V^o_{pl} is taken to be 21.09 cm^3, and the mass of the plenum structure m_{pl} is estimated at 85.5g. The fuel mass m_f is assumed to be half the mass of the active fuel in the pin, added to the mass of the blanket fuel, for a total of 155 g.

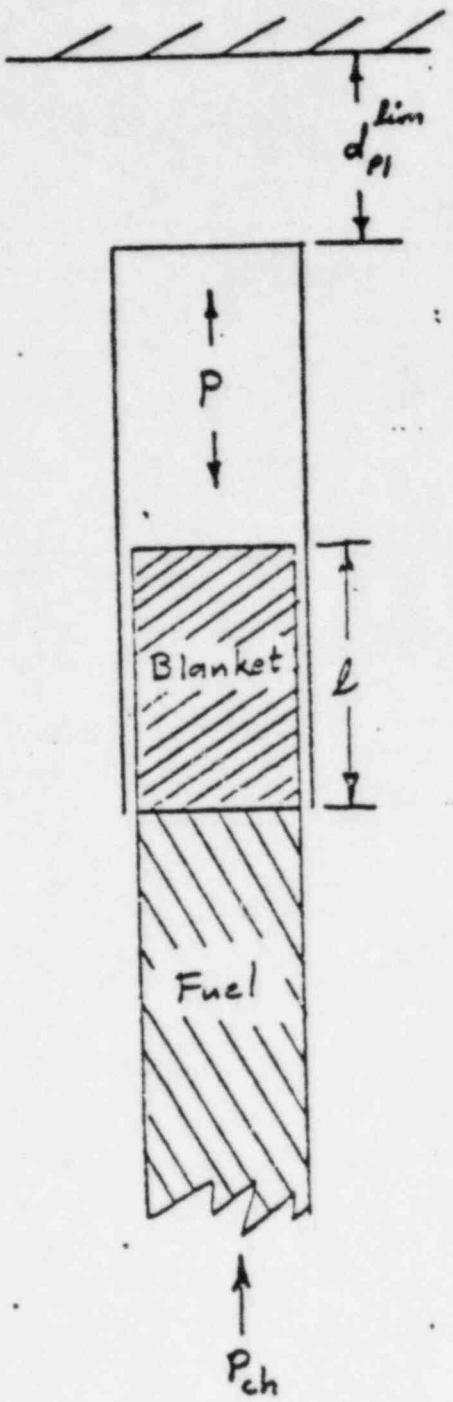

Figure D1. Assumed Simplified Geometry of the Pin Stub and Plenum Region

Fuel motion is calculated as a result of the forces due to gravity,

$$F_g = m_f \cdot g \ , \tag{3}$$

and due to the excess of the plenum pressure P over the channel pressure P_{ch},

$$F_p = \pi r^2 (P - P_{ch}) \ , \tag{4}$$

where r is the fuel-pellet radius, taken to be 0.254 cm.

The acceleration of the fuel is calculated from the total force,

$$a_f = \frac{F_g + F_p}{m_f} \ , \tag{5}$$

and integrated over small time steps Δt to obtain the downward velocity

$$v_f \cong v_f^i + a_f \Delta t \ , \tag{6}$$

where v_f^i is the velocity at the beginning of the time step.

The downward displacement is obtained by calculating the displacement increment in the time step, using the mean velocity for the time step;

$$d_f \cong d_f^i + (v_f^i + \frac{a_f \Delta t}{2}) \Delta t \ . \tag{7}$$

A parallel calculation is carried out for the upper pin structure, with the difference that the gas pressure and gravity act in opposite directions. Upper movement of the pin structure is limited to an arbitrary (input) value, so that the effect of restraint can be considered.

The plenum pressure is recalculated for each time step, to reflect the reduction due to the escape of plenum gas, and the reduction due to the increase in plenum volume due to the relative motion of the pin structure and the fuel. Initially, the calculated value of β may be smaller than the critical value for choked flow, calculated to be 0.13516 for this problem. When this situation does occur, the critical value is used for β.

The extent to which the upper pin structure can move upward is not clear, but subassembly schematics from CRBR PSAR[39] suggest that a large fraction of the pins can move a considerable distance. Given the fact that the wire wraps can unravel, and the fact that any motion would likely start from the subassembly center and progress outward, it would appear that significant upward motion of the pin structure could take place. If this motion is unimpeded, the finite-difference calculations indicate that the plenum pressure will be released in 0.027s.

It should be noted that the function multiplying P on the right-hand side of equation 1 varies slowly during the blowdown; β is small, while the parameter F is about 25. As a result, the pressure decay is about exponential, of the form

$$P = P_o \exp(-t/\tau) .$$

The time "constant" is defined from equation 1 as

$$\tau = \left[\left(\frac{RT}{Z} \right)^{1/2} \frac{Ag}{V} \left(\frac{1 - \beta^2}{F - \ell n \beta} \right)^{1/2} \right]^{-1}$$

This blowdown time is the time required for the pressure to fall to 1/e of its initial value. Even though τ is not constant, its value is useful in estimating the blowdown rate. The initial value of τ for the present calculations, at 1200K, is about 0.25s. This value is based on a constant gap width of 0.0143 cm and a flow length of 35.56 cm.

Appendix E

Modified Treatment of Partial Clad Blockages in the SAS3D Boiling Model

After the formation of partial blockages in the coolant channel, due to the motion of molten clad, the coolant boiling model sometimes tends to calculate negative pressures in the middle of a blockage. These negative pressures, in addition to being unphysical, cause the program to become numerically unstable and terminate. The problem is due to an acceleration term in the momentum equation for the vapor. For the current CRBR and R8 cases, this acceleration term was modified to give a solution that is physically more meaningful and numerically more stable.

In SAS3D the momentum equation for sodium vapor contains an acceleration term of the form

$$\frac{d}{dz}\left(\frac{G^2}{\rho}\right).$$

If the flow area changes due to the motion of molten clad, then the code uses a term of the form

$$\frac{1}{A}\frac{d}{dz}\left(\frac{AG^2}{\rho}\right),$$

where G is the mass flux in the vapor, ρ is the vapor density, A is the coolant flow area, and z is the axial position. In case of a large vapor flow through a local partial blockage involving a large area change, this term contributes little or nothing to the over-all pressure drop across the blockage, since the pressure loss on one side of the blockage is largely

cancelled by pressure recovery on the other side; but in the middle of the blockage this term tends to drive the pressure negative. In such cases, a rapid drop in the pressure in the blockage leads the code to cut back the coolant time step to very small values in an attempt to obtain an accurate and stable solution; but the tendency toward negative pressures often causes the code to go unstable and terminate. Therefore, the code was modified so that the acceleration term is eliminated at any node interval where the coolant flow area is less than 56% of the nominal value, or at any time when the coolant time step is cut to less than 3×10^{-5} seconds. Pressure drop through the blockage is always accounted for by the friction term, which can get large if the flow area is small.

REFERENCES

1. Letter HQ:S:82:110 John Longenecker, to Paul Check, Amend. No. 72 to the PSAR for CRBRP, dated Oct 29, 1982

2. S. K. Rhow, et. al., "An Assessment of HCDA Energetics in the CRBRP Heterogeneous Reactor Core," CRBRP-GEFR-00523 (December, 1981).

3. T. E. Kraft, "An Evaluation of Recent Transient Fuel Behavior Models Based on Selected Experimental Results," ANL/RAS 80-29 (November, 1980).

4. J. M. Kramer, et. al., "An Analysis of Recent Fuel Disruption Experiments," Intl. Top Mtg. on LMFBR Safety, Lyon, France (July, 1982).

5. E. E. Gruber and E. H. Randklev, "Comparison of Fission Gas Effects in a Transient Overpower Test (HUT 5-7A) to FRAS3 Code Predictions," Intl. Top. Mtg. on Fast Reactor Safety Technology, Seattle, Washington (August, 1979).

6. R. Simms, et. al., "TREAT Experimental Data Base Regarding Fuel Dispersals in LMFBR Loss-of-Flow Accidents," Proc. of Top. Mtg. on the Reactor Safety Aspects of Fuel Behavior, Sun Valley, Idaho (August, 1981).

7. R. Simms, et. al., "Loss-of-Flow TREAT Tests L6 and L7 with Irradiated LMFBR-Type Fuel", Nucl. Tech., 52, 331 (March, 1981).

8. R. Simms, "An Evaluation of Fuel Motion in Recent TREAT Experiments with Liquid-Metal Fast Breeder Reactor Fuel," Nucl. Tech., 50, 257 (October, 1980).

9. W. R. Bohl, "SLUMPY: The SAS3A Fuel Motion Model for Loss-of-Flow," ANL/RAS 74-18 (August, 1974).

10. B. W. Spencer, et.al., "Final Report on TREAT Tests R4 and R5; Seven-Pin, Loss-of Flow Tests with Full-Length Unirradiated FFTF-Type Fuel Pins," ANL-79-106 (December, 1979).

11. B. W. Spencer, et. al., "Interim Report on TREAT Test R8, a Seven-pin Loss-of Flow Test with Pressurized Pins", ANL/RAS 78-39 (September, 1978).

12. T. E. Kraft, et. al., "Final Report on the SLSF In-Pile Experiment P3A", ANL/RAS 81-20 (June, 1981).

13. T. E. Kraft, et. al., "SLSF In-Reactor Experiment P3 Interim Posttest Report", ANL/RAS 78-53 (December, 1978).

14. C. W. Hunter, R. L. Fish, and J. J. Holmes, "Mechanical Properties of Unirradiated Fast Reactor Cladding During Simulated Overpower Transients," Nucl. Tech., 27, (1975).

15. C. W. Hunter, G. D. Johnson, and R. L. Fish, "Mechanical Properties During Simulated Overpower Transients of Fast Reactor Cladding Irradiated from 700-1000 F," HEDL-TME 75-28, Hanford Engineering Development Laboratory, Richland, WA (June, 1975).

16. G. D. Johnson and C. W. Hunter, "Mechanical Behavior of Fast Reactor Fuel Pin Cladding Subjected to Simulated Overpower Transients," HEDL TME 78-13 (June, 1978).

17. Letter, M. L. Hamilton, HEDL, to A. Biancheria, W-ARD, D. B. Atcheson, GE, and G. D. Johnson, "Transmittal of FCTT Data Base for Cladding Failure Criteria," March 9, 1982.

18. D. R. Duncan, G. D. Johnson, and C. W. Hunter, "Effects of Multiple Transients on Fast Reactor Fuel Pin Cladding Mechanical Properties," Trans. Am. Nucl. Soc., 30, p. 196, (Nov., 1978).

19. N. S. Cannon and C. W. Hunter, "Transient Undercooled Overpower (TUCOP) Simulation on Fast Reactor Cladding," HEDL TC-2260, (Sept., 1982).

20. H. U. Wider, et. al., "The PLUTO-2 Overpower Excursion Code and a Comparison with EPIC," Proc. Int'l Mtg. on Fast Reactor Safety, Seattle, Washington, (August 1979).

21. H. U. Wider and L. A. Semenza, "Analysis of TREAT Transient Overpower Experiments Using the PLUTO Codes," Proc. Specialists Workshop on Predictive Analysis in LMFBR Safety, Los Alamos, New Mexico, LA-7938-C (March, 1979).

22. D. L. Graff, "Results of Testing and Validation Efforts on the Two-Fluid (TWOFLU) Hydrodynamics Module of TRANSIT-HYDRO," ANL/RAS 82-32 (October, 1982).

23. D. L. Graff and J. E. Cahalan, "Modified ICE Technique for Two-Phase Systems with Strong Mass Sources," Trans. Am. Nuc. Soc., 39, 505 (1981).

24. D. P. Weber, "The VENUS-III HMT Algorithm: A Non-linear Implicit Eulerian Hydrodynamics Algorithm for Two-fluid Models without Slip," ANL/RAS 79-5 (April, 1979).

25. T. J. Scale, et. al., "OPERA Fifteen-Pin Sodium Expulsion Test," Trans. Am. Nuc. Soc., 43 (1982).

26. W. R. Bohl and T. J. Heames, "CLAZAS: The SAS3A Clad Motion Model," ANL/RAS 74-15 (August, 1974).

27. W. R. Bohl, "CLAP: A Cladding Action Program for LMFBR HCDA LOF Analysis," Trans. Am. Nucl. Soc., 23, p. 348 (1976).

28. M. Ishii, W. L. Chen, and M. A. Grolmes, "Multichannel Model for Relocation of Molten Fuel Cladding in Unprotected Loss-of-Flow Accidents in Liquid Metal Fast Breeder Reactors," Nuc. Sci. Eng., 69 (1979).

29. W. L. Chen and M. Ishii, "A Parametric Study of Multichannel Molten Cladding Motion Under Unprotected Loss-of-Flow Accident Conditions in LMFBR's," Nuclear Engineering and Design, 61, No.3 (December, 1980).

30. J. E. Cahalan, et. al., "A Preliminary User's Guide to Version 1.0 of the SAS3D LMFBR Accident Analysis Computer Code," Reactor Analysis and Safety Division Internal Report, Argonne National Laboratory (July, 1977).

31. T. G. Theofanous, M. DiMonte, and P. D. Patel, "Incoherency Effects in Clad Relocation Dynamics for LMFBR CDA Analyses," Nuc. Eng. Design, 36 (1976).

32. G. B. Wallis, One-Dimensional Two-Phase Flow, McGraw-Hill, New York (1969).

33. G. D. Johnson and C. W. Hunter, "Mechanical Properties of Transient-Tested Irradiated Fast Reactor Cladding," Trans. Am. Nucl. Soc., 30, p. 195, (Nov., 1978).

34. J. M. Kramer and R. J. DiMelfi, "An Analysis of the Rupture Behavior of Fast Reactor Fuel Cladding Subjected to Thermal Transients," J. Eng. Mat'ls. and Tech., 101., 293-298 (1979).

35. J. M. Kramer and R. J. DiMelfi, "Modeling Deformation and Failure of Fast Reactor Cladding During Simulated Accident Transients," Nucl. Eng. and Des., 63, 47-54 (1981).

36. R. J. Dimelfi and J. M. Kramer, "Modeling the Transient Failure Behavior of Irradiated Fast Reactor Cladding Tubes Including Fuel-Adjacency Effects," Trans. of the 6th Int. Conf. on Structural Mechanics in Reactor Technology, Paris, France, August 17-21, 1981 paper C3/3.

37. F. E. Dunn, et. al., "The SAS2A LMFBR Accident-Analysis Computer Code," ANL-8138 (October, 1974).

38. T. C. Chawla, G. M. Hauser, M. A. Grolmes, and H. K. Fauske, Nucl. Sci. Eng. 58, 21-32 (1975).

39. Chapter 4.2 of the CRBRP Preliminary Safety Analysis Report, Project Managemer Corporation, Docket No. 50-537, 1978.

Enclosure 5

This enclosure contains the response to item 8 of enclosure 1.